Generation of diversity in the blue cheese moldPenicillium roquefortiand identification of pleiotropic QTL for key cheese-making phenotypes

Thibault Caron, Ewen Crequer, Mélanie Le Piver, Stéphanie Le Prieur, Sammy Brunel, Alodie Snirc, Gwennina Cueff, Daniel Roueyre, Michel Place, Christophe Chassard, et al.

Generation of diversity in the blue cheese mold *Penicillium roqueforti* and identification of pleiotropic QTL for key cheese-making phenotypes

Thibault CARON[1,3,$], Ewen CREQUER[1,2,$], Mélanie LE PIVER[3], Stéphanie LE PRIEUR[1], Sammy BRUNEL[3], Alodie SNIRC[1], Gwennina CUEFF[2], Daniel ROUEYRE[3], Michel PLACE[3], Christophe CHASSARD[5], Adeline SIMON[6], Ricardo RODRIGUEZ DE LA VEGA[1], Monika COTON[2], Emmanuel COTON[2], Marie FOULONGNE-ORIOL[4*], Antoine BRANCA[1,7*], Tatiana GIRAUD[1*],

1: Ecologie Systématique Evolution, IDEEV, Bâtiment 680, 12 route RD128, Gif-sur-Yvette, France

2: Univ Brest, Laboratoire Universitaire de Biodiversité et Ecologie Microbienne, F-29280, Plouzané, France

3: Laboratoire Interprofessionnel de Production – SAS L.I.P., 34 rue de Salers, Aurillac, France

4: INRAE, MycSA, Mycologie et Sécurité des Aliments, 33882 Villenave d'Ornon, France

5: Université Clermont Auvergne, INRAE, Vetagro Sup, UMRF, 20 Côte de Reyne, Aurillac, France

6: Université Paris-Saclay, INRAE, UR1290 BIOGER, Palaiseau, France

7: Université Paris-Saclay, CNRS, IRD, UMR Évolution, Génomes, Comportement et Écologie, 91190 Gif-sur-Yvette, France

*These authors jointly supervised the study.

$These authors contributed equally to this work.

Corresponding author: Ewen Crequer <Ewen.Crequer@univ-brest.fr>; "Tatiana Giraud" <tatiana.giraud@universite-paris-saclay.fr>;

Keywords: genetic map, filamentous fungi, translocation, chromosomal rearrangements, breeding, yeast, food, Starship

Abstract

Elucidating the genomic architecture of quantitative traits is essential for our understanding of adaptation and for breeding in domesticated organisms. *Penicillium roqueforti* is the mold used worldwide for the blue cheese maturation, contributing to flavors through proteolytic and lipolytic activities. The two domesticated cheese populations display very little genetic diversity, but are differentiated and carry opposite mating types. We produced haploid F1 progenies from five crosses, using parents belonging to cheese and non-cheese populations. Analyses of high-quality genome assemblies of the parental strains revealed five large translocations, two having occurred via a circular intermediate. Offspring genotyping with genotype-by-sequencing (GBS) revealed several genomic regions with segregation distortion, possibly linked to degeneration in cheese lineages. We found transgressions for several traits relevant for cheese making, with offspring having more extreme trait values than parental strains. We identified quantitative trait loci (QTLs) for colony color, lipolysis, proteolysis, extrolite production, including mycotoxins, but not for growth rates. Some genomic regions appeared rich in QTLs for both lipid and protein metabolism, and other regions for the production of multiple extrolites, indicating that QTLs have pleiotropic impacts. Some QTLs corresponded to known biosynthetic gene clusters, e.g., for the production of melanin or extrolites. F1 hybrids constitute valuable strains for cheese producers, with new traits and genetic diversity, and allowed identifying target genomic regions for traits important in cheese making, paving the way for strain improvement. The findings further contribute to our understanding of the genetic mechanisms underlying rapid adaptation, revealing convergent adaptation targeting major regulators.

Introduction

Most traits of agricultural or evolutionary significance are quantitative and genetically complex, involving multiple genes that interact with one another and the environment (Falconer and Mackay 1995). Genomic loci showing diversity associated with quantitative trait variation are called QTLs, for "quantitative trait loci". Domesticated species are good models for understanding the genomic architecture of quantitative traits involved in adaptation. Indeed, they have been subjected to recent and strong selection on known traits, and display highly contrasting phenotypes compared to wild populations, as well as between different domesticated varieties. In addition to the fundamental interest in understanding the genomic basis of adaptive changes, the agronomically important traits targeted for genetic improvement generally follow quantitative inheritance.

In the QTL mapping approach, genotyping and phenotyping of progenies allow assessing statistical associations between genotypes and phenotypes, thereby allowing identifying genomic regions affecting traits of interest (Falconer and Mackay 1995). The QTL approach has largely advanced our understanding of the genomic architecture of important traits, for example in crops and cattle (Adamczyk et al. 2013; Silva et al. 2014; Kumar et al. 2017). Studies of the genomic architecture of adaptation in crops have revealed that traits involved in domestication were often controlled by only a few QTLs with pleiotropic effects, often being major regulators (Sweeney and McCouch 2007; Baach et al. 2008; Bachlava et al. 2010; Wang et al. 2010; Telias et al. 2011; Wirén and Jensen 2011; Andargie et al. 2014; Johnsson et al. 2014; Wright 2015; Wright et al. 2015; Kongjaimun et al. 2012; Kantar et al. 2017; Somta et al. 2020; Bomblies and Doebley 2006; Martìnez-Ainsworth and Tenaillon 2016). The most emblematic example is the *teosinte branched 1 (tb1)* locus in maize, that determines apical dominance as well as other domestication traits, which is due to a transposable element insertion in a regulatory region (Doebley et al. 1997; Martìnez-Ainsworth and Tenaillon, 2016).

Domesticated fungi used for food production, such as *Saccharomyces cerevisiae* for fermentation, filamentous fungi for cheese maturation or the button mushroom *Agaricus bisporus* for direct human consumption, also represent good models for understanding the genomics of adaptation, in particular

as they have small and compact genomes (Gladieux et al. 2014). QTL mapping proved to be an efficient tool for identifying the genes affecting phenotypes impacting technological performances of industrial yeast strains, such as thermotolerance, chemical resistance, dehydration stress tolerance, and phenotypes associated with the fermentation process, such as volatile compounds production, ethanol production, in nitrogen-limited fermentations and in nitrogen consumption and utilization (Nguyen *et al.* 2022; Kessi-Pérez et al. 2020; Eder *et al.* 2018; Wilkening *et al.* 2014; Swinnen, Thevelein and Nevoigt 2012; Liti and Louis 2012; Steinmetz *et al.* 2002). In addition to classic QTLs, traits have also been reported to be impacted in yeasts by aneuploidy (Todd, et al. 2017) and genomic rearrangements (Zimmer *et al.* 2014). QTL mapping has also been successfully used in *A. bisporus,* for identifying the genomic regions controlling color and spore number (Foulongne-Oriol et al. 2012; Imbernon et al. 1996), in the causal agent of the cereal disease *Fusarium* head blight, *Fusarium graminearum*, for identifying the genetic determinants of aggressiveness (Laurent et al. 2021), and in the *Lachancea waltii* yeast, for identifying genomic regions controlling the growth rate in the presence of various drugs (Peltier et al. 2021).

Penicillium roqueforti is the mold used for the maturation of all types of blue cheeses worldwide, responsible for the typical blue-veined aspect, and contributing to their specific flavor and aroma, in particular through high levels of proteolytic and lipolytic activities (Moreau 1980; Cerning et al. 1987; Collins et al. 2003). When this study was performed, four populations had been identified in *P. roqueforti*, two populations being used to produce cheeses and two populations being found in molded silage and lumber or in spoiled food (Dumas et al. 2020). The two populations used for cheese maturation each show footprints of bottlenecks and a domestication syndrome, with phenotypes contrasting with those of the non-cheese populations and beneficial for several important aspects of cheese safety, appearance and flavor (Dumas et al. 2020; Caron et al. 2020; Crequer et al. 2023). The two cheese populations each correspond to a clonal lineage, with contrasted phenotypes and diversity levels, and inoculated in different types of cheeses, *i.e.* Roquefort PDO (protected designation of origin) versus other blue cheeses (Gillot et al. 2015; Dumas et al. 2020). The *P. roqueforti* cheese

96 populations produce cheeses with higher percentages of blue area and with higher quantities of desired
97 volatile compounds than non-cheese populations (Caron et al. 2020).

98 The Roquefort population, found in Roquefort PDO cheeses, displays some level of genetic diversity
99 and exhibits traits beneficial for pre-industrial cheese production, *e.g.* slower growth in cheese models
100 and greater spore production on bread, the traditional multiplication medium (Gillot et al. 2017;
101 Dumas et al. 2020). The Roquefort population also produces higher quantities and more diverse
102 positive aromatic compounds in cheeses, which is due to its faster and different proteolysis and
103 lipolysis activities (Caron et al. 2020; Dumas et al. 2020). In addition, the Roquefort population
104 produced cheese with lower water activity, which could restrict spoiling microorganisms (Caron et al.
105 2020). Lipolysis and proteolysis are important traits in *P. roqueforti*, involved in cheese maturation,
106 yielding the specific volatile and metabolic compounds responsible for the desired strong and spicy
107 blue cheese flavors (Cerning et al. 1987; Collins et al. 2003; Gillot et al. 2017).

108 The other cheese population, named non-Roquefort, is constituted by a single clonal lineage, due to a
109 recent strong selection for a single "performant" strain, and is found in all types of blue cheese
110 worldwide except Roquefort PDO cheeses. The non-Roquefort population display phenotypes more
111 suited for industrial cheese production, such as a more efficient cheese cavity colonization ability,
112 higher tolerance to salt, to acidic pH and to lactic acid compared to other populations (Dumas et al.
113 2020; Ropars et al. 2020; Crequer et al. 2023), and the production of volatiles important for aroma and
114 flavor, *e.g.* methyl ketones (Caron et al. 2020). The non-Roquefort clonal lineage acquired large
115 genomic regions by horizontal transfers (Dumas et al. 2020; Ropars et al. 2015), mediated by giant
116 Starships mobile elements (Gluck-Thaler et al. 2022). These horizontally transferred regions include in
117 particular two very large regions called *Wallaby* and *CheesyTer*, which encompass genes with
118 functions in lactose metabolism or competition against other microorganisms. The non-Roquefort
119 lineage further displays footprints of positive selection in genes involved in volatile compound
120 production (Dumas et al. 2020) and has lost the ability to secrete the mycophenolic acid (MPA)
121 mycotoxin, an immunosuppressant used for preventing transplant organ rejection (Matas et al. 2013),
122 because of a deletion in a key gene (*mpaC*) of its biosynthesis pathway (Gillot et al. 2017; Crequer et

al. 2024). *Penicillium roqueforti* can secrete other metabolites, *i.e.* extrolites, including some considered as toxins (*e.g.* Roquefortine C and PR toxin), but not found in blue cheeses, or in such low concentration that they do not cause acute health hazards (Scott, 1981; Fontaine et al. 2015; Hymery et al. 2017). Other *P. roqueforti* extrolites can be of interest, such as the potential antitumor compounds andrastin A and (iso)-fumigaclavine A (Ge et al. 2009; Matsuda et al. 2013). These active compounds may be used by the fungus in the competition against other microorganisms (Jakubczyk et al. 2020; Conrado et al. 2022), and thus avoid cheese spoilage, although little is known on these aspects.

Identifying the genomic regions controlling the phenotypes contrasting between the four *P. roqueforti* populations thriving in different niches would have important fundamental implications for our understanding of the genomic architecture of adaptation and also applied consequences for strain improvement by marker-assisted selection in progenies. However, because of the clonal population structure of the two domesticated cheese lineages, it is not possible to identify the genetic determinants of important traits for cheese making through phenotype/genotype association without producing a recombinant population, which would also allow generating genetic and phenotypic diversity from the two single clonal lineages used in most blue cheeses worldwide (Dumas et al. 2020). Fortunately, sexual reproduction can be induced in *P. roqueforti* (Ropars et al. 2014), the two cheese lineages carry opposite mating types, and some strains have retained some level of sexual fertility, despite the general degeneration in sexual reproduction ability in the cheese populations (Ropars et al. 2016). As the life cycle of *P. roqueforti* has a dominant haploid phase, direct access to this phase allows association genetics to be carried out on first-generation offspring.

Here, we therefore aimed at generating diversity in cheese *P. roqueforti* populations and at identifying the genomic regions controlling the phenotypic differences between the non-Roquefort and Roquefort lineages, and more generally between *P. roqueforti* populations. For this goal, we produced five sexual F1 haploid progenies by crossing six fertile haploid *P. roqueforti* strains from the four originally identified populations at the beginning of the study, focusing particularly on the cross between the two cheese populations, Roquefort and non-Roquefort. We studied in the progenies several phenotypes important for cheese making, *i.e.* lipolysis, proteolysis, growth, color and the production of the main

known extrolites: roquefortine C and PR toxin, with its intermediates eremofortins A and B, as well as metabolites with lower toxicity risk, *i.e.* andrastin A, (iso)-fumigaclavine A and MPA (Coton et al. 2020; Chàvez et al. 2023). Depending on the desired cheese product, different values may be wanted for the various traits analyzed. For example, slower growth, lipolysis and proteolysis may allow to store cheeses longer without product degradation, while faster lipolysis may contribute to stronger aromas and faster growth to bluer cheeses (Caron et al. 2020). We analyzed 1,073 offspring with single nucleotide polymorphisms (SNPs) obtained using genotype-by-sequencing (GBS). Because genotyping revealed the presence of the two parental alleles in some genomic regions in the otherwise haploid offspring, we also generated high-quality genome assemblies for the parental strains, to compare the parental genomes and identify genomic translocations. We built genetic maps and ran QTL analyses to identify the genetic architecture of the phenotypes important for cheese making.

Results

Five fertile crosses involving at least one cheese strain

We chose the five most fertile crosses among 17 trials involving in each case at least one cheese strain. We identified the isolated spores that were actually recombinant ascospores and not asexual conidia by using 11 microsatellite markers. We focused on the cross between the two cheese populations, *i.e.* Roquefort (R) and non-Roquefort (N), as it may be the most interesting for strain improvement in the cheese making context, and we isolated 387 recombinant offspring (Table 1). The other crosses each involved a cheese strain (either R or N) and a strain from a non-cheese population, either silage (S) or lumber/food spoiler populations (L), and we isolated between 157 and 185 recombinant offspring for each of these four crosses (Table 1).

Transgression and heterosis in phenotype distributions

We measured several phenotypes important for blue cheese production, *i.e.*, mycelium growth, colony color, lipolysis, proteolysis and extrolite production. We analyzed nine variables summarizing these traits in the five progenies, plus seven traits related to extrolite production in three crosses, resulting in

66 trait distributions (9x5+7x3). Among these 66 distributions, 28 did not significantly deviate from normality, 10 best fitted a unimodal distribution and 30 a bimodal distribution (Supplementary Figures 1 and 2; Supplementary Table 1). None of the phenotype distributions were trimodal or amodal (Supplementary Table 1).

The distribution of the five progenies on the principal component analysis based on trait values (Supplementary Figure 3) shows that they represent overall a higher phenotypic diversity than each cross considered separately. A few traits appeared positively or negatively correlated (Figure 1 D), some associations being expected, such as between color traits (*e.g.* blue and red) or between the production of different targeted extrolites (Marcano et al. 2023; Torrent et al. 2017; Rojas-Aedo et al. 2018; Gillot et al. 2017). Other associations were more surprising, such as the negative correlation between proteolysis rate on the one hand, and green and hue level on the other hand (Figure 1 D).

We found heterosis in the progenies, computed as the difference in mean trait values between the parents and their progenies (Supplementary Table 2). Out of the 66 phenotype distributions, 53 displayed significant positive or negative heterosis. We found negative heterosis in all crosses for the production of PR toxin (the most toxic *P. roqueforti* mycotoxin) and andrastin A, indicating that progenies produced on average less of these two extrolites than their parent mean, which can be beneficial for cheese making. In contrast, we found positive heterosis in all crosses for MPA production, a less toxic extrolite. All tested phenotypes exhibited both positive and negative transgressions across all crosses, *i.e.* with some offspring displaying higher values and others lower values than either parent, which holds promise for the generation of phenotype diversity and strain improvement. We found a large proportion of offspring with low or no PR toxin production in the RxN and SxN crosses. We detected in all crosses negative transgression in roquefortine C production level (*i.e.* the offspring mean was lower than the parental mean) and many offspring with no MPA production, which is promising for the selection of hypotoxinogenic strains.

High values of phenotype heritability

Narrow-sense heritability (h^2) represents the part of phenotypic variance explained by additive genetic variance, *i.e.* the part on which selection can act. The narrow-sense heritability of growth rate, lipolysis, proteolysis and color across the five progenies, estimated by regressions of the progeny trait means on the parent trait means, were relatively high, with for example two-thirds of traits with h^2 above 30% (Table 3). Some estimates were below zero or higher than 100% (Figure 1), but narrow-sense heritability estimates based on regressions between offspring and parent trait means may not be highly reliable with only five crosses, and even only three crosses in the case of the targeted extrolites. For extrolite production, we also estimated broad-sense heritability (H^2) as we measured two replicates for each strain (Supplementary Table 3). The broad sense heritability estimates for extrolite production were high, ranging between 91.3 % for roquefortine C and 99.6% for isofumigaclavine A, which is promising for selection (Supplementary Table 3).

Translocations between parental genomes

The comparison of high-quality genome assemblies revealed five large genomic chromosomal rearrangements between the parents in four crosses (LxN, RxN, RxS, RxL; Figure 2), which had impacts on genetic maps. These translocations ranged from 60 to 530 kb in size. The two silage parents and the non-Roquefort parent showed syntenic genomes between each other, suggesting that they kept the ancestral arrangement order. We could therefore infer that four of the translocations (L1, L2, L3 and L4) occurred in the lumber population while the fifth one, R1, occurred in the Roquefort population (Figure 2). We detected no particular transposable element family or clusters at the margin of the translocations or DUF domains specific to Starship elements.

The L1 and L4 regions displayed internal rearrangements between their copies in different genomic locations: the last 3' portion of each of the L1 and L4 regions in the parents with the ancestral arrangement was located in 5' of the L1 and L4 regions in the translocated parent (Supplementary Figure 4). This internal rearrangement suggests that the translocation occurred via a circular intermediate mechanism, with an insertion cutting site in each of the L1 and L4 regions different from their excision site (Supplementary Figure 4).

Both parental alleles for the R1 region insertion were found together in 38, 31 and 24 % of the RxN, RxL and RxS offspring in GBS data, respectively (Figure 2). The Oxford Nanopore long-read mapping depths confirmed the presence of two R1 region copies in the six analyzed offspring from the RxN cross with both R1 region parental alleles detected in GBS data. Similarly, the long-read mapping confirmed that the five offspring with a single parental allele in GBS data carried a single copy of the translocated region in their genomes. The absence of this translocated region is likely lethal as we did not detect any offspring with no R1 copy, while some recombination events should have generated offspring with none of the two copies. We detected no offspring with both parental alleles nor an absence of the region for the translocations L1 to L4, indicating that both the duplication or absence of these regions lead to inviability.

We checked that the presence of the two R1 copies in haploid genomes was stable after culture and replication of 24 offspring of the RxN cross carrying the two parental alleles. After cultivating these 24 offspring from the RxN cross for one week on plates and transferring conidia from the edge of the colony to new plates 19 times, PCRs showed that the cultivated lineages still carried the two R1 parental alleles. We did not detect any RIP footprints (C-to-T repeat-induced point mutations) in the R1 regions of the six offspring with a duplicated R1 region and with high-quality genome assemblies. However, RIP footprints would only be expected in the following generation (F2), after a sex event involving genomes with the duplicated region, as RIP is known to occur during the short dikaryotic phase of sexual reproduction in ascomycetes (Galagan and Selker 2004).

Genetic maps, recombination pattern and segregation biases

We identified between 2,462 and 2,943 reliable markers in the progenies across the five crosses, evenly distributed along the non-Roquefort reference genome. For constructing genetic maps, we excluded redundant markers, *i.e.* those physically close and with identical segregation patterns in a given cross. We thus constructed the genetic maps with 1,448 markers for the RxN cross, and 676 to 785 markers for the other crosses with fewer analyzed offspring (Table 2). The genetic maps for the five crosses displayed lengths between 775 and 913 cM, with a mean of 857 cM (Table 2). We

detected four linkage groups in each genetic map, corresponding to the four chromosomes in the parental genome assemblies (Figure 3). The mean number of crossing-overs per chromosome was 2.15, with a maximum of 2.58 for chromosome 1, the longest chromosome, and a minimum of 1.25 for chromosome 4, the smallest chromosome. The mean recombination rate was estimated between 27.0 cM/Mb and 31.8 cM/Mb, with a mean of 29.8 ± 1.8 cM/Mb (Table 2). The LxN cross had a particularly low mean recombination rate, mainly due to the presence of two cold spots of recombination on chromosome 1 (indicated by a plateau in the plot of genetic map positions against genomic positions; empty rectangles in Figure 3), with local recombination rates of 6.7 cM/Mb and 3.1 cM/Mb, respectively (Table 2). The edges of the two cold spots corresponded to the translocated regions in the chromosome 1 of the LCP06039 strain (regions L1, L2, L3, Figure 2 and 3). This is likely due to the inviability of offspring carrying either zero or two copies of the translocated region because of recombination events between their insertion sites (Figure 2). Other regions with low or no recombination rates corresponded to horizontally transferred regions only present in the reference genome, putative centromeres, other translocated regions and TE-rich regions (Figure 2 and 3).

In the five crosses, large regions presented segregation biases, with under-representation of alleles from the cheese populations (*i.e*. either from the Roquefort or non-Roquefort parents; Figure 4). Such segregation biases could allow the purge of deleterious mutations in the cheese clonal lineages, but could also render the selection of valuable alleles that are in linkage with deleterious alleles in these regions more challenging. The segregation bias against the non-Roquefort parent allele in the second half of chromosome 4 (between 3.5Mb and 4.2Mb) was present in all crosses involving the non-Roquefort parent (Figure 4) and was very strong (>90% of the alternative allele in all three crosses). Such strong under-representation of alleles from the cheese population in all of these three crosses can be due to the lower fertility of domesticated populations (Ropars et al. 2016), with likely deleterious alleles accumulated through clonal replication that lead to low viability of the ascospores carrying them. We observed another segregation bias with strong over-representation (> 90%) of silage parental alleles, in the RxS and SxN crosses, in chromosome 1 from 4.2 to 4.5Mb (Figure 4). The under-represented allele, that of the cheese parents, displayed no segregation bias in the other crosses

involving the cheese parents (Figure 4), suggesting the presence of either a selfish element (*e.g.* a spore killer) or a highly beneficial allele for early growth in the corresponding region in the silage/spoiled food parents rather than a deleterious one in the cheese parent. This interpretation is supported by the over-representation of the silage allele in two different crosses and the lack of bias in the RxL and LxN crosses in this region, while these observations would not be expected if the cheese parents had deleterious alleles in this region. The segregation bias with over-representation of Roquefort alleles at the end of chromosome 1 is likely due to the lack of the R1 translocated region that leads to offspring inviability. Symmetrically, the alleles from the other parent tended to be over-represented at the R1 locus on chromosome 2, but not significantly so. This suggests that the location of R1 may be more advantageous on chromosome 1 than on chromosome 2.

Detection of QTL with pleiotropic effects

We investigated QTLs for the nine traits associated with lipolysis, proteolysis, growth and color in all descendants, as well as for the seven traits associated with extrolite production specifically in the RxN, RxL and SxN crosses (Supplementary Table 4). We found QTLs for all tested phenotypes except for growth rate (Figure 4; Supplementary Table 4), indicating that marker-assisted selection for these traits may be performed for strain improvement and diversification. We detected 123 QTLs across all phenotypes and crosses, 109 explaining more than 5% of the variance (hereafter called “major QTLs”). We identified 58 major QTLs for the eight parameters related to lipolysis, proteolysis and color, across the five crosses, with 8 to 17 QTLs per cross, with a mean of 1.3 major QTLs and a maximum of 3 major QTLs per trait and cross. For extrolite production, we identified 13 to 23 major QTLs across the three progenies analyzed for these traits, with a mean of 2.4 and a maximum of 5 major QTLs per extrolite and cross (Supplementary Table 4, Figure 4).

The identified QTLs and the direction of their effects were in agreement with the past occurrence of selection for color, proteolysis, lipolysis and extrolite production in cheese populations. We indeed identified QTLs impacting colony color, bluer colonies being associated with cheese parent alleles, and in particular in the genomic region containing the dihydroxynaphthalene-melanin biosynthesis

306 cluster, known to be involved in melanin production (Figure 4). The cheese parent alleles were also
307 both associated with slower proteolysis and faster lipolysis, in connection with firmer texture and
308 longer cheese storage and the production of typical blue cheese flavors, respectively. We identified
309 QTLs for the production of three extrolites, MPA, PR toxin and roquefortine C, the non-Roquefort
310 alleles being associated with lower production levels (Figure 4). This is consistent with a selection for
311 bluer color, more efficient lipolysis and less efficient proteolysis in domesticated lineages, as well as
312 lower extrolite production levels.

313 Most of the major QTL regions presented pleiotropic effects. The 109 major QTLs were indeed not
314 distributed homogeneously across the genome, with instead regions carrying clustered QTLs for
315 different phenotypes (Figure 4, Supplementary Figure 5). We considered as pleiotropic the regions
316 presenting overlaps in QTL regions of at least two different trait classes in a given cross (proteolysis,
317 lipolysis, color and extrolite production). We identified five such regions, among which three regions
318 displayed pleiotropic impact on the four trait classes, *i.e.* proteolysis, lipolysis, color and extrolite
319 production, across the different progenies, and also within some progenies for multiple traits (empty
320 vertical rectangles in Figure 4, Supplementary Figure 5). For the pleiotropic region on chromosome 2,
321 the Roquefort allele was associated with faster lipolysis and lower proteolysis. This QTL region
322 displayed significant interactions for lipolysis with two other QTLs, in chromosomes 3 and 4; such
323 interactions between loci in determining a trait value constitute positive epistasis. The same region
324 also impacted color. For the pleiotropic regions detected in chromosomes 1 and 3, the non-Roquefort
325 alleles were associated with slower proteolysis, faster lipolysis and bluer colony color (Supplementary
326 Table 4, Figure 4). We further found epistasis for other types of phenotypic traits, particularly between
327 different QTLs controlling proteolysis (Supplementary Table 4, Figure 4). QTL interactions had the
328 same sign (positive or negative) across the various crosses in some cases and different signs in other
329 cases, indicating that epistatic interactions are dependent on the genetic background. Such epistasis
330 could impair selection, as recombination breaks up allelic combinations, while specific allelic
331 combinations are beneficial under positive epistasis.

We also identified QTLs for extrolite level production, including some outside of their known biosynthesis gene clusters, suggesting that these QTLs correspond to *trans*-acting regulators. For three extrolites (MPA, PR toxin and roquefortine C), we identified QTLs with intervals included in their biosynthesis cluster, with non-Roquefort alleles associated with lower production levels. The lower MPA production level associated with the non-Roquefort allele is likely due to the deletion in the *mpaC* gene that was identified in the non-Roquefort population (Gillot et al. 2017; Crequer et al. 2024). We also found a QTL in a region including the PR toxin biosynthesis gene cluster, with lower production level of the PR toxin but accumulation of its production intermediates, eremofortins A and B, associated with the non-Roquefort allele at the PR toxin biosynthesis cluster. This suggests a disruption in the cluster driving low production levels of the toxin and accumulation of its intermediates in offspring presenting the non-Roquefort allele likely due to a premature STOP codon in the ORF11 gene of the cluster (Crequer *et al.* 2024). The offspring harboring a non-Roquefort allele for the various biosynthesis gene clusters displayed lower production levels of the two most toxic *P. roqueforti* extrolites, *i.e.* PR toxin and roquefortine C, and of the less toxic MPA extrolite, which is consistent with a selection for an hypotoxinogenicity trait in the non-Roquefort population (Fontaine *et al.* 2015; Hymery *et al.* 2017; Crequer *et al.* 2024). Most of the QTLs associated with extrolite production were not located within their biosynthesis gene cluster, which suggests the implication of *trans*-acting regulators. These QTLs were often shared between different extrolites, suggesting a co-regulation of their pathways, which could facilitate the selection for low extrolite production in strains bred for cheese production. In particular, isofumigaclavine A production shared five of its eight major QTLs with andrastin A production, suggesting co-regulation of the production of the two extrolites. We detected QTLs for all tested extrolites, except roquefortine C, in the R1 region for its two insertion sites (Figure 4), with lower production associated with the presence of the R1 region. Such a QTL clustering suggests the presence of a master regulator of extrolite production in the R1 region. We in fact found an ortholog of a master regulator gene in the R1 region, namely the *srk1* gene, regulating osmotic and oxidative responses in fungi (Marquina *et al.* 2022). The selection of offspring with two R1 regions could thus allow further decreases in overall extrolite content, and in particular that of the studied mycotoxins in cheese.

We detected an andrastin A QTL next to the *Wallaby* horizontally transferred region (HTR) in the RxN cross and a proteolysis QTL in the region containing the *CheesyTer* HTR in each of the SxN and LxN crosses (Figure 4). Multiple other phenotypes have previously been suggested to be controlled by these HTRs, such as milk sugar metabolism and interactions with other microorganisms (Ropars *et al.* 2015), but the indel nature of these HTRs may render hard to detect their associations with phenotypes, as markers are lacking in one of the parents.

We also checked whether QTL regions encompassed other regulators known to be involved in extrolite production (*prlaeA,* Marcano *et al.* 2023, *pcz1,* Gil-Durán *et al.* 2015, and *sfk1*, Torrent *et al.* 2017) as well as other essential phenotypes in *P. roqueforti*, such as conidiation or growth rate. We located *pcz1* in the pleiotropic region of chromosome 2, encompassing QTLs for andrastin A production and color, melanin being involved in both color and conidiation (Gil-Durán *et al.* 2015); *pcz1* could therefore be a candidate for the QTLs controlling andrastin A production and color via expression regulation. While no QTL interval overlapped with *prlaeA*, a QTL region controlling MPA production in one cross encompassed *sfk1*. However, this QTL region overlaps with a shorter MPA QTL present in another cross without *sfk1* in the confidence interval, which suggests no implication of *sfk1* in MPA production regulation.

The QTL intervals were too large to identify particular genes or functions beyond the horizontal gene transfers, biosynthesis gene clusters of the targeted extrolites or other *a priori* candidate genes. Indeed, with on average one gene every 3kb in the annotated Roquefort parental strain and a median QTL length of 760 kb, half of the QTL regions are expected to encompass more than 250 genes. We therefore only tried to identify candidate genes in the smallest QTL intervals explaining more than 20% of the phenotypic variance. We found an enrichment in genes involved in carbohydrate catabolism for a QTL associated with color in the pleiotropic region of chromosome 2 (g3621 to g3634), and a pepsin gene (endopeptidase, g5778) for a QTL associated with proteolysis in chromosome 3. Carbohydrate catabolism and pepsin are of paramount importance for secondary starters, to use the remaining lactose residues to establish themselves early in the cheese matrix

(Cerning *et al.* 1987), and to degrade caseins and therefore to participate in proteolysis (Grippon *et al.* 1977), respectively.

Discussion

In this study, we aimed at generating genetic and phenotypic diversity in the blue cheese fungus *P. roqueforti* by analyzing haploid F1 progenies from five crosses between cheese or non-cheese strains, and identifying QTLs for key traits in cheese making. This will be essential for both strain breeding purposes and for studying the genomic architecture of traits selected during domestication. Generating diversity and reshuffling alleles is crucial as deleterious mutations have accumulated in the two clonal lineages currently used for cheesemaking. Moreover, their low diversity raises concern for the sustainable use of *P. roqueforti* for cheese making. We successfully generated offspring by crossing strains from different populations of *P. roqueforti*, despite the known low fertility of the cheese populations (Ropars *et al.* 2016). The progenies displayed a broad diversity for the phenotypes important for cheese making, in terms of growth, color, proteolysis and lipolysis rates, as well as extrolite production, with more extreme trait values than the parents. We detected QTLs for all these traits except growth, often displaying pleiotropic effects. These findings will be highly valuable for strain breeding, and further suggests that humans have domesticated this cheese fungus by selecting major regulators, as reported in crops (Telias *et al.* 2011; Wirén & Jensen, 2011; Wang *et al.* 2010; Sweeney & McCouch, 2007; Wright, 2015; Wright *et al.* 2015; Baach *et al.* 2008; Johnsson *et al.* 2014; Bachlava *et al.* 2010; Andargie *et al.* 2014; Kongjaimun *et al.* 2012; Kantar *et al.* 2017; Somta *et al.* 2020; Bomblies & Doebley, 2006; Martìnez-Ainsworth & Tenaillon, 2016).

Variability in phenotypes in progenies, with heterosis and positive transgression for most traits

We found large phenotypic variation, transgression and heterosis in progenies for multiple relevant phenotypes for blue cheese production, *i.e.* mycelium growth, lipolysis, proteolysis and extrolite production. Progenies displayed transgression, with the trait values of some offspring being much more extreme than those of the parents. All progenies also exhibited heterosis, indicating mean trait values in offspring that may be better than the mean value of the parents. Both transgression and

heterosis are promising for strain improvement and diversification. Furthermore, we detected QTLs for most traits, indicating that selection is possible, and even marker-assisted selection. The generation of variation is particularly important in *P. roqueforti*, as the two main cheese populations, Roquefort and non-Roquefort, have lost most of their genetic diversities due to recent bottlenecks followed by strong selection in industrialization times (Dumas *et al.* 2020). These clonal lineages even degenerate in terms of sexual fertility and probably for other traits of interest for cheese making (Ropars *et al.* 2016). Sexual reproduction is the only way to purge deleterious mutations that accumulate during clonal propagation. The progeny between the Roquefort and non-Roquefort strains is particularly promising, as a European regulation requires a food safety assessment ("Novel food" law; UE No 2015/2283) for the use of microorganisms for food production except if they have already been used for food before May 1997. The cross of parental strains already used for cheese production for decades should therefore meet the European Union requirements. The other crosses may also be of great interest, even for the European market, as the regulation might be interpreted in terms of species rather than strains, as already done for example in wine and beer yeasts.

Translocations and segregation biases

The obtained high-quality genome assemblies led to the identification of five translocations between the parental strains, having occurred independently in three lineages. We also identified offspring carrying twice the R1 rearranged region. For these translocations, we did not find any offspring completely lacking them, indicating that their absence in genomes may lead to offspring unviability. For the L1, L2, L3, and L4 translocations, we detected no offspring with twice the regions either, implying that their duplications are also lethal. We detected lower production levels for the targeted metabolites in offspring carrying two copies of the R1 region. These offspring may therefore be highly valuable for cheese making, especially as the presence and locations of the translocations were stable through multiple replications and culture events. For further improvement, it should however be checked that future crosses with these offspring will not induce RIP in the duplicated region. RIP footprints (*i.e.* mutations from CA to TA in repeated sequences) have indeed been already detected in *P. roqueforti* (Cheeseman & Ropars *et al.* 2014).

We detected no particular transposable element types or abundance at the margin of the translocations. In particular, we detected no DUF3435 domain, typical of Starship elements, that move within and between fungal genomes via a circular intermediate (Bucknell & MDonald, 2023) and are involved in horizontal gene transfers in *P. roqueforti* (Gluck-Thaler et al. 2022). Nevertheless, the L1 and L4 translocations appeared to have occurred via a circular form. These regions may therefore correspond to a new type of large mobile element with a circular intermediate. These findings reinforce the view that fungal genomes are highly dynamic, with frequent gene movements, within genomes, between individuals or even between species, and that this contributes to adaptation (Bucknell & MDonald, 2023).

For several translocated regions, either their lack or duplication in genomes led to to unviability, which induced the cosegregation of the two insertion sites, potentially generating linkage drag in future breeding, *i.e.* cosegregation of desired and undesired alleles in progenies. For other translocated regions, only their absence was lethal, and this led to segregation biases in progenies. We detected additional segregation biases, in other genomic regions, mostly with under-representation of the parental strain from the parental domesticated cheese populations. Such biases are likely due to degeneration in the cheese clonal lineages, with alleles less fit than in the wild populations, especially under sexual reproduction and ascospore germination (Ropars *et al.* 2016). We detected a strong segregation distortion in chromosome 4, with an absence of the non-Roquefort alleles in the progeny. This suggests an unviability of the ascospores carrying the non-Roquefort allele, in agreement with the low fertility of the non-Roquefort population, showing high post-mating sterility, *i.e.* formation of cleistothecia without ascospores (Ropars *et al.* 2016). The region with segregation distortion in chromosome 4 contained two orthologs of genes involved in sporulation in the *Saccharomyces cerevisiae* yeast, g9043 and g9061 coding for SPS22-like (Coluccio *et al.* 2004) and RMD1-like proteins (inferred by electronic annotation, UniprotKB-KW; Enyenihi & Saunders, 2003), suggesting that the region contains genes essential for sexual reproduction. The region with segregation distortion in chromosome 4 also included genes with premature stop codons in the non-Roquefort parent, although with either no predicted function or a function with *a priori* no relationship with sexual

reproduction (g8973 and g8998). In the case of the RxS and SxN segregation bias in chromosome 1, the under-represented Roquefort and non-Roquefort alleles displayed no segregation bias in the other crosses involving the same Roquefort and non-Roquefort parents. This indicates that the bias depends on the genetic background and may therefore be due to epistatic interactions leading to a deleterious effect or a selfish meiotic drive element (Grognet *et al.* 2014; Turner & Perkins, 1979).

QTL identification and the genomic architecture of adaptation

We identified QTLs for all phenotypes but growth, confirming that selection of these traits for strain improvement can be considered. There were only a few major QTLs per trait and cross, which should facilitate strain breeding. The QTLs for color, lipolysis and proteolysis on the one hand, and for extrolite production on the other hand, clustered in the same genomic regions, suggesting pleiotropy, or clustering of genes with effects on these different pathways. The three pleiotropic regions affecting color, and lipid and protein degradation have the same effects, with faster lipolysis, slower proteolysis and bluer colony color for the cheese strain allele. This is consistent with a selection for a bluer color, stronger flavors and a longer conservation in domesticated lineages of *P. roqueforti* for cheese making. Furthermore, such pleiotropy or gene clustering may render selection for these traits easier or more challenging depending on whether alleles coding for desired and unwanted traits are associated. Actually, pleiotropic regions controlling multiple important traits for cheese making may be the result of human selection targeting major regulators, and their finding informs on the genomic architecture of adaptation. The control of traits involved in domestication by only a few QTLs and their pleiotropy have been reported in animals and plants, often due to major transcription regulators, human selection having targeted “masterminds” (Martìnez-Ainsworth & Tenaillon, 2016), but also to the genetic determinant of important crop traits being clustered in genomes (Wright, 2015; Kantar *et al.* 2017). Here, we show that such pleiotropic regions are present in two independently domesticated lineages of *P. roqueforti*, with the same type of effect on the phenotype, suggesting evolutionary convergence (Ropars & Giraud, 2022) and selection of major regulators with pleiotropic effects.

Known shared regulators of various secondary metabolites include *prlaeA*, *sfk1* and *pcz1*, their silencing or knock-out decreasing the production of roquefortine C, andrastin A et MPA (Marcano *et al.* 2023; Torrent *et al.* 2017; Rojas-Aedo *et al.* 2018). Over-expression of *pcz1* decreases the production of roquefortine C and andrastin A, and increases the production of MPA; *pcz1* also impacts growth, conidiation and spore germination (Gil-Durán *et al.* 2015); *pcz1* was found in one of the pleiotropic regions with an impact on andrastin A production and on color, which is mostly due to conidia pigmentation.

In addition, we found QTL regions containing the biosynthesis gene clusters involved in PR toxin, MPA and roquefortine C production. In the RxS and LxN crosses, we found a QTL affecting the colony color in a region containing the DHN melanin biosynthesis gene cluster, known to code for the production of *P. roqueforti* conidia pigment (Cleere *et al.* 2024; Seekles *et al.* 2021). Besides these *a priori* candidates, the QTL analysis did not point to particular genes or regulatory regions, as the regions with significant impacts were large, encompassing many genes, which impaired searching for relevant gene functions. Furthermore, as shown in plant domestication, several important traits have evolved due to transposable element insertions in regulatory regions (Martìnez-Ainsworth & Tenaillon, 2016; Yao *et al.* 2015), in which case approaches based on gene functions may not be powerful.

QTLs for desired traits in Penicillium roqueforti

We observed a large diversity of phenotypes within each of the generated progenies compared to current commercial strains, and an even greater diversity across the five progenies. We detected pleiotropic regions, acting on multiple metabolism traits, which could facilitate or impair the selection for desired combinations of lipolysis, proteolysis and color. The presence of additional QTLs elsewhere in the genome suggests that a finer selection could be possible for one of the traits without affecting the others. Therefore, our study paves the way for strain improvement and diversification in cheese-making strains.

Toxin production is a concern in *P. roqueforti*, in particular the production of PR toxin and roquefortine C. The low toxin concentrations found in cheese and the long history of safe consumption of blue cheeses, combined with the recent discovery that both Roquefort and non-Roquefort populations are unable to produce PR toxin, indicate the innocuity of commercial strains in cheese production (Crequer *et al.* 2024). Nevertheless, selecting strains with even lower toxin production would be of major interest. We found several QTLs with effects on extrolite production. In particular, QTLs in the biosynthesis gene clusters of PR toxin, roquefortine C and MPA indicated that the corresponding non-Roquefort alleles decreased extrolite production. This suggests selection for lower toxicity in the domesticated non-Roquefort lineage. In addition, lower production of several extrolites was associated with the duplication of the R1 region. Selection of these alleles could thus further improve the safety of *P. roqueforti* use in cheese production or for new products such as vegan cheese. While toxin production is detrimental for cheese safety, other extrolites can be interesting to produce for medical applications: for example, MPA is an immunosuppressant used for preventing transplant organs rejection (Matas *et al.* 2013), and andrastin A, a potential antitumor compound (Ge *et al.* 2009; Matsuda, Awakawa & Abe, 2013). Our study shows large positive transgression for the production of these extrolites and multiple QTL regions. These results are highly promising to increase their production level in the pharmaceutical context.

We detected QTLs for color as well as for protein and lipid degradation. In blue cheeses, lipolysis and proteolysis by *P. roqueforti* influence texture, taste and the production of aromatic compounds, the latter being mainly influenced by lipolysis (Cantor *et al.* 2004). Currently, the texture and the amount of aromatic compounds in the final product is mostly controlled by the length of the ripening period. A longer ripening time increases the duration of lipolysis and proteolysis in cheeses, leading to a softer texture and the production of more pronounced aromatic compounds in the final product (Cantor *et al.* 2004). Although the general consumer demand is moving towards milder products (Michel Place, L.I.P. S.A.S. pers. com.), producers aim to develop a range of products with varying degrees of flavor to meet the diversity of consumer preferences (*i.e.* product segmentation). For example, the Carles firm producing Roquefort PDO cheeses generated a new strain (called “Maxime”) producing milder

cheeses, with lighted blue color, called “Elegance” (https://www.professionfromager.com/salon-virtuel/france/occitanie/article/carles). Another interest of producers is the visual aspect of the cheese, which depends on the initial color of the spores and the ability of the strain to maintain this color in conditioned atmospheres (Fairclough, Cliffe & Knapper, 2011). We identified QTLs for these traits, indicating that selection for strain improvement and diversification should be possible, for example the selection of strains with different colors, and proteolysis or lipolysis activities.

Breeding could thus be performed in *P. roqueforti* using crosses between different populations and then back-crosses to retain only the desired new traits while purging deleterious mutations. It would thus be possible to use the QTLs identified here for marker-assisted selection, as done in *Saccharomyces cerevisiae* for malic consumption (Vion *et al.* 2021). As *Penicillium roqueforti* is haploid, there is no issue of inbreeding depression and selection is particularly efficient, as there is no dominance effect of masking alleles. Marker-assisted selection is all the more useful in *P. roqueforti* as the assessment of cheese features requires a long and time-consuming process of cheese making with multiple replicates in controlled environments (Caron *et al.* 2021).

Conclusion

In this study, we managed to generate F1 offspring from different crosses, including one between parents from the two domesticated cheese populations, and obtained high variability in phenotypes in progenies. This is crucial given the very low diversity currently available in each of the Roquefort and non-Roquefort cheese populations. Despite genomic rearrangements and segregation biases due to deleterious alleles, the QTL approach identified regions involved in important traits for cheese making. The high heritabilities and the QTLs identified for all traits but growth indicate that selection should be efficient for strain improvement. Segregation biases, linkage drag, pleiotropy and genomic rearrangements may however reduce the efficacy of selection.

Further efforts could increase the number of offspring and use the Termignon cheese population recently discovered in non-inoculated French cheeses produced at a small scale in the Alps, as this population is genetically and phenotypically differentiated from the two other cheese populations

(Crequer *et al.* 2023). With a better understanding of the demands of consumers and cheese producers, association genetics could become a very promising tool for the improvement of *P. roqueforti* strains, increasing blue cheese quality and diversity. Few studies have addressed these questions in the domestication of fungi so far, beyond yeasts and the button mushroom (Foulongne-Oriol *et al.* 2012; Imbernon *et al.* 1996; Nguyen *et al.* 2022; Kessi-Pérez, Molinet & Martínez, 2020; Eder *et al.* 2018; Wilkening *et al.* 2014; Swinnen, Thevelein & Nevoigt 2012; Liti & Louis, 2012; Steinmetz *et al.* 2002). From a fundamental point of view, identifying the genomic regions controlling traits of interest to humans helps understand the genetic mechanisms behind the adaptation of organisms to their environment. In particular, our findings of similar QTLs between independently domesticated *P. roqueforti* lineages, with pleiotropic effects, indicate convergent adaptation targeting major regulators.

Materials and methods

Progeny production

The production of progenies was obtained following the protocol in Ropars *et al.* (2014) with some modifications. Six *P. roqueforti* strains (Table 1) were selected for their fertility as observed in a previous study (Ropars *et al.* 2016) and based on their phenotypic differences estimated from proteolysis and lipolysis measurements (Dumas *et al.* 2020). They were crossed in all possible pairs given their mating types, either MAT1-1 (three strains) or MAT1-2 (three strains) (Table 1).

For each cross, three Petri dishes were inoculated on an oat medium supplemented with biotin after sterilization (6.4 µg/L; Böhm *et al.* 2012). On each Petri dish, 5 µL of an uncalibrated spore suspension was used to inoculate agar sections at opposite sites on the Petri dish, located perpendicular to the sections inoculated with aliquots of conidia of the opposite sexual type (Figure 5 A; O'Gorman, Fuller & Dyer, 2009). Petri dishes were sealed with food-grade plastic film and incubated upside down at 19°C in the dark. The contact zone between strains (Figure 5 A) was examined with a binocular loupe and an optical microscope regularly for four to six weeks to check for the presence of cleistothecia (sexual structures). When cleistothecia were found, three to five of them were sampled,

598 crushed with tweezers, and observed under an optical microscope with lactophenol cotton blue dye
599 solution for ascospore detection (Figure 5 B and C). We took the pictures with a Nikon DS-Fi2
600 camera, on an inverted optical microscope with apodized phase contrast (Nikon France, Champigny-
601 sur-Marne, France). When ascospores were identified, all the cleistothecia of the corresponding Petri
602 dish were collected in a 0.05% Tween-20 water suspension (P1379-100mL Sigma Aldrich, Saint
603 Quentin Fallavier, France). Because cleistothecia are covered with conidia derived from asexual
604 reproduction, we developed a treatment to kill them before releasing ascospores from cleistothecia.
605 Approximately 500 µL of the cleistothecia suspension was pooled with 500 µL of a commercial 2.6%
606 sodium hypochlorite solution and gently agitated for 20 seconds; then 1 mL of water was added to stop
607 the sodium hypochlorite action. Cleistothecia were washed twice with one-minute centrifugation at
608 7,000 rpm, removal of the supernatant and resuspension in Tween 20. Then, we crushed cleistothecia
609 with a sterile piston (Piston Pellet Eppendorf, Montesson, France) and filtered residues with a 40 µm
610 filter (cell screen, Greiner, Les Ulis, France). Single-ascospore isolation was carried out with a dilution
611 method on malt extract agar Petri dishes (MEA, Galloway and Burgess 1952).

612 **Recombinant offspring detection**

613 We chose five fertile crosses for further analyses (Table 1). Genomic DNA was extracted from fresh
614 mycelium and conidia suspension after single-ascospore isolation and growth for five days on MEA
615 media using the Nucleospin soil kit (Macherey-Nagel, Düren, Germany). For checking that isolated
616 spores were recombinant offspring and not asexual conidia, we used 11 microsatellite markers (Ropars
617 *et al.* 2014) labeled with fluorescence, out of which between five and nine were polymorphic
618 depending on the cross. These markers were amplified with the Multiplex PCR kit (Qiagen, Les Ulis,
619 France) using a touchdown program with an initial denaturation of 15 min at 95°C, 35 cycles of 30 s at
620 94°C, a decrease of 1°C every 90 s from 60 to 50°C, and 60 s at 72°C. The PCR program ended with a
621 final 30 min extension step at 60°C. Genotyping by capillary fractionation electrophoresis was
622 performed at INRAe Clermont-Ferrand (INRAe Platform GENTYANE, Clermont-Ferrand,
623 FRANCE). The profiles obtained were analyzed with the GENEMAPPER v4.0 software (Applied
624 Biosystem, Villebon-sur-Yvette, France) to detect recombination between parental genotypes. Only

strains with recombinant genotypes were retained, *i.e.* carrying alleles from one parent at some markers and alleles for the other parent at other markers.

Genome sequencing, assembly and analysis

We generated long-read-based genome assemblies by sequencing the genomes of the LCP06136 parental strains, as well as 24 F1 offspring, with Oxford Nanopore MinION technology with an R9 flow cell, a high-quality genome assembly of the other parental strain (LCP06133) being available (Crequer *et al.* 2023). We also generated genome assemblies for the other parents, based on Illumina sequencing and assemblies guided by the Oxford Nanopore assemblies of the LCP06136 and LCP06133 parents.

DNA was extracted from mycelium and conidia with the Nucleospin soil kit for the progeny and with the NucleoBond High Molecular Weight DNA kit (Macherey-Nagel, Düren, Germany) for the parental strain LCP06136, with mechanical disruption of about 30 mg of lyophilized mycelium with two tungsten beads (3 mm diameter) for 5 min at 30 Hz. The Nanopore library was prepared with the SQK-LSK109 ligation sequencing kit, starting with 1.5 µg DNA, and sequencing was performed in-house with a MinION combined with a MinIT (version 19.06.9), a 72 hour run, and with the Fastcalling basecalling algorithm. The genome of the LCP06136 strain was sequenced alone in a R9 flow cell, whereas the 24 offspring genomes were sequenced in a 12-plex with the Rapid Barcoding Sequencing kit SQK-RBK004. We assessed run quality using Porechop v0.2.3_sequan2.1.1 (Wick *et al.* 2017), and when necessary, demultiplexed the Nanopore raw reads with the default parameters.

De novo assemblies of the genomes were constructed from both Illumina and Nanopore reads. For the LCP06136 parental genome, the raw Nanopore reads were trimmed and assembled with Canu v1.8 (Koren *et al.* 2017) with the option genomeSize=28m. The assembly obtained with Canu was polished twice with Illumina reads (Dumas *et al.* 2020) using Pilon v1.24 (Walker *et al.* 2014) with the default settings. For each round of polishing, Bowtie2 (Langmead and Salzberg, 2012; Langmead *et al.* 2019) was used to align the Illumina trimmed reads with the assembly for polishing with a maximum length (-X) of 1000bp. The Illumina reads were first trimmed with Trimmomatic v0.36 (Bolger, Lohse &

Usadel, 2014) with the following options: ILLUMINACLIP:TruSeq3-PE.fa:2:30:10 LEADING:10 TRAILING:10 SLIDINGWINDOW:5:10 MINLEN:50. Redundant contigs were removed based on a self-alignment using NUCmer version 3.1 (Kurtz *et al.* 2004). For other parental strains (LCP06037, LCP06039, LCP06043, LCP06059), available Illumina reads (Dumas *et al.* 2020) were trimmed with Trimmomatic v0.36 (Bolger et al 2014) the same way as previously described, and assembled with SOAPdenovo2 v2.04 (Luo *et al.* 2012) using the corresponding default size 23 k-mer length. The assemblies obtained were then scaffolded using Ragout v2.3 with the LCP06136 and the LCP06133 genomes as references (Kolmogorov *et al.* 2018). For the 24 offspring genomes, the raw Nanopore reads were trimmed and assembled both with Canu v1.8 (Koren *et al.* 2017) and with Flye version 2.9 (Kolmogorov *et al.* 2019), and then merged using Quickmerge (Solares *et al.* 2018). The merged assemblies obtained were polished once with a concatenation of Illumina reads of the parental strain LCP06136 and LCP06133 (Dumas *et al.* 2020) in the same way as for the LCP06136 parental genome. The obtained assemblies were scaffolded using Ragtag v2.1.0 (Alonge *et al.* 2022). We evaluated the quality of the final assemblies with Quast v5.0.2 (Gurevich *et al.* 2013) and their completeness with BUSCO v5.3.2 (Manni *et al.* 2021) using the eurotiales_odb10 lineage dataset. Based on the quality and completeness, we selected 11 out of the 24 offspring strain assemblies for further analyses.

Transposable elements (TEs) were annotated using the REPET package (https://urgi.versailles.inra.fr/Tools/REPET). The TEdenovo pipeline (Flutre *et al.* 2011) was used to detect repeated elements in LCP06136 and LCP06133 (https://doi.org/10.57745/SIP7CH) genomes, and to provide consensus sequences. These consensus sequences were classified with PASTEC v1.3 (Hoede *et al.* 2014), based on the Wicker hierarchical TE classification system (Wicker *et al.* 2007) and manually curated. The resulting bulk library of consensus sequences was then used to annotate TE copies in the six whole genomes (namely, LCP06136 and LCP06133, LCP06037, LCP06039, LCP06043, LCP06059) using the TEannot pipeline (Quesneville *et al.* 2005). Repeat-induced point mutations (RIP) in assemblies were detected using the web-based tool The RIPper (Van Wyk *et al.* 2019).

All final assemblies were formatted (contigs being renamed and ordered in descending order of size), and repeats of the LCP06133 and LCP06136 parental genomes were masked with RepeatMasker v4.1.2 (Smit et al 2013) after *de novo* repeat detection using RepeatModeler v2.0.2 (Smit and Hubley 2008). We performed gene annotation on the masked assemblies of the parental strain LCP06136 using the Funnannotate v1.8.9 pipeline (Palmer and Stajich 2020), with Braker v2.1.6 (Brůna *et al.* 2021; Hoff et al. 2016; Hoff *et al.* 2019; Stanke *et al.* 2006; Stanker *et al.* 2008), which uses a combination of the *ab initio* gene predictors Augustus and GeneMark-ET (Lomsadze et al. 2014) with NCBI blast (Altschul *et al.* 1990) and blast+ (Camacho *et al.* 2009). We ran BRAKER twice, first using the BUSCO dataset of proteins eurotiales_odb10 (Manni *et al.* 2021) with the ProtHint pipeline (Brůna et al. 2020; Buchfink et al. 2015; Gotoh et al. 2014; Iwata and Gotoh, 2012; Lomsadze *et al.* 2005), and then using the RNA-seq dataset from Punt *et al.*(2020) and mapped using STAR v2.5.4b (Dobin *et al.* 2013) with the default settings. We combined the results of the two BRAKER runs with TSEBRA (the Transcript Selector for BRAKER; https://github.com/Gaius-Augustus/TSEBRA).

We studied synteny between assemblies by investigating collinearity of one-to-one orthologs along whole genome alignments, using nucmer v3.1 (Kurtz *et al.* 2004), with 500pb as the minimum match length. We visualized synteny between genomes by plotting one-to-one ortholog links using Circos v0.69-6 (Krzywinski *et al.* 2009).

Phenotyping

We selected four traits for their applied interest in cheesemaking that are easily measurable with precision and at high throughput, for which we assessed the phenotypes in all the isolated offspring obtained for the five analyzed crosses. The growth rate was measured using a ScanStation (Interscience, Mourjou, France), an incubator for temperature-controlled growth (set at at 22.5°C) taking pictures regularly for each of 100 Petri dishes as well as analyzing images. We spread 5 µL of standardized spore suspension (250 spores/inoculation) on each Petri dish, containing malt medium (Biokar BK045 HA) at 15 $g.L^{-1}$ in source water (Cristalline, Chelles, France), sterilized at 120°C during 15 minutes. The ScanStation took pictures of the Petri dishes right side up on a black

704 background, for five days every 30 minutes, *i.e.* 240 measures per strain (Figure 5 D). The ScanStation
705 estimated the colony area and diameter for each picture, by counting the number of pixels
706 corresponding to the fungal colony. Because the colony diametral growth was near linear when plotted
707 against days (Supplementary Figure 6), we used, as a measure of growth rate, the slope of the least
708 square linear regression computed with the *lm* function of the base package R software v4.3.2
709 (http://www.r-project.org/). The coefficients of determination (r^2), measuring the fit of the data to a
710 line, are presented in the Supplementary Table 5 and the linear regression of an offspring with a
711 median r^2 in the Supplementary Figure 6. To ensure the robustness of the linear fit, strains with
712 coefficients of determination below 0.98 were not considered in the QTL analysis of this trait (21 of
713 885, *i.e.* 2.4% of strains filtered out).

714 The colony color was measured after growth on raw sheep milk powder medium (Biocoop, Paris,
715 France) at 21% in source water, sterilized at 105°C for five minutes, and mixed with 1.7% agar in
716 source water, sterilized at 121°C for 15 minutes. After 13 days of growth, two pictures were taken by
717 the ScanStation under standardized conditions of light and on a white background (Figure 5 F). We
718 recorded for each strain the colony color decomposition using RGB (red, green and blue) and HSB
719 (hue, saturation, and brightness) with ImageJ v1.52n (Schneider 2012; Supplementary Table 6). In the
720 RGB system, the levels of red, green and blue are represented by a range of integers from 0 to 255
721 (256 levels for each color). In the HSB system, hue ranges from 0 to 360 (0 is red, 120 is green, 240 is
722 blue), saturation and brightness from 0 to 100% (0% saturated is neutral grey, 100% saturated is the
723 full color ; 0% brightness is black, 50% brightness is normal, 100% brightness is white). In order to
724 obtain uncorrelated components from the RGB data, we divided each value by the sum of the three
725 components. For each of these parameters, we recorded average values across all the colony pixels for
726 each strain. For QTL detection, we chose *a posteriori*, among these color parameters, those whose
727 distributions and heritabilities were optimal for QTL analysis (*i.e.* largest and uncorrelated variance);
728 we thus retained the RGB proportion, as well as HSB.

729 The lipolytic and proteolytic activities of *P. roqueforti* strains were measured *in vitro* following
730 Dumas *et al.* (2020): for each strain, 50 µl of standardized spore suspensions (ca. 2,500

spores/inoculation) were inoculated at the top of a test tube containing agar and tributyrin for lipolytic activity measure (10 $mL.L^{-1}$, ACROS Organics) or semi-skimmed cow milk for the proteolytic activity measure (40 $g.L^{-1}$, Casino). The lipolytic and proteolytic activities were estimated by the degree of compound degradation, which changes the media from opaque to translucent. We measured the distance between the initial mark and the hydrolyzed, translucent front, after 7, 14, 21 and 28 days of growth at 20°C in the dark (Figure 5 E). As lipolysis curves were nearly linear when plotted against days, we estimated the lipolysis rate with a linear regression computed with the R base package function *lm*. Proteolysis profiles appeared less linear but with no clear sigmoid nor other regression patterns, so we also chose to fit linear models for more simplicity. The coefficients of determination (r^2), measuring the fit of the data to a line, are presented in the Supplementary Table 5 and an example of a linear regression of an offspring with a median r^2 in the Supplementary Figure 6.

For extrolite production, we grew fungal cultures in 24-well sterile microplates containing 2 mL of yeast extract sucrose (YES) agar medium buffered at pH 4.5 with phosphate-citrate buffer and characterized by a high C/N ratio to favor extrolite production as previously described (Frisvad & Filtenborg, 1983). For each strain, 1 µL of a calibrated spore suspension (10^6 $spores.mL^{-1}$) prepared from a 7-day culture was inoculated in the centre of the well. Two replicates per strain were performed for extrolite analyses. The plates were incubated at 25°C in the dark for seven days and then stored at -20°C until extrolite analysis. For extrolite extractions, we used an optimized “high-throughput” extraction method (Lo *et al.* 2023; Crequer *et al.* 2024). Briefly, 2g-aliquots (the entire YES culture obtained from a well) were homogenized after thawing samples with a sterile flat spatula then 12.5 mL of acetonitrile (ACN) supplemented with 0.1% formic acid (v/v) was added, samples were vortexed for 30 sec followed by 15 min sonication. Extracts were again vortexed before being centrifuged for 10 min at 5000g at 4°C. The supernatants were directly collected and filtered through 0.45 µm PTFE membrane filters (GE Healthcare Life Sciences, UK) into amber vials and stored at -20°C until analyses. Extrolite detection and quantification were performed using an Agilent 6530 Accurate-Mass Quadropole Time-of-Flight (Q-TOF) LC/MS system equipped with a Binary pump 1260 and degasser, well plate autosampler set to 10°C and a thermostated column compartment. Filtered 2 µL aliquots

were injected into a ZORBAX Extend C-18 column (2.1x50 mm and 1.8 µm, 600 bar) maintained at 35°C with a flow rate set to 0.3 $mL.min^{-1}$. The mobile phase A contained milli-Q water + 0.1% formic acid (v/v) and 0.1% ammonium formate (v/v) while mobile phase B was ACN + 0.1% formic acid. Mobile phase B was maintained at 10% for 4 min, followed by a gradient from 10 to 100% for 18 min. Then, mobile phase B was maintained at 100% for 5 min before a 5-min post-time. Samples were ionized in positive (ESI+) electrospray ionization modes in the mass spectrometer with the following parameters: capillary voltage 4 kV, source temperature 325°C, nebulizer pressure 50 psig, drying gas 12 $L.min^{-1}$, ion range 100-1000 m/z. Target extrolite characteristics used for quantifications are given in Supplementary Table 7 and included commercially available extrolites produced by *Penicillium* species, namely andrastin A, eremofortins A & B, (iso)-fumigaclavin A, mycophenolic acid and roquefortine C. Andrastin A, eremofortins A & B and (iso)-fumigaclavin A standards were obtained from Bioviotica (Goettingen, Germany), while all others were from Sigma-Aldrich (St Louis, MO, USA). All stock solutions were prepared in dimethyl sulfoxide (DMSO) at 1 $mg.mL^{-1}$ in amber vials. As the PR toxin was not commercially available, a previously produced purified stock solution (Gillot *et al.* 2017) without known concentration was used to ensure MPA (mycophenolic acid) and PR toxin were separated (as they have the same mass) as well as linearity of PR toxin quantification. For these analyses, metabolite identification was performed using both the mean retention time ± 1 min and the corresponding ions listed in Supplementary Table 7. We used a matrix-matched calibration curve (r^2 >0.99 for all extrolites except 2 >0.96) to confirm linearity the relation between signal area and extrolite concentration with final concentrations ranging from 1 to 10000 $ng.mL^{-1}$ according to the target metabolite and method performance was carried out as previously described (Gillot *et al.* 2017).

Statistical analysis on phenotypes

For phenotype distributions, we performed tests of normality with the *shapiro.test* function of the base package of R software v4.3.2 (http://www.r-project.org/). We ran tests for unimodality with the *dip.test* function of the Diptest package v0.75-7 (Maechler 2016) and tests for bimodality with the *bimodality_coefficient* function of the Mousetrap package v3.2.1 (Kieslich *et al.* 2019) with a threshold of 0.555 according to Pfister *et al.* 2013. We performed the trimodality and amodality tests

785 with the *is.trimodal* and *is.amodal* functions, respectively, of the LaplacesDemon v16.1.6 package
786 (Hall *et al.* 2021). We computed the average heterosis as ((F1 - MP) / MP) * 100, F1 and MP being the
787 trait mean values of the progeny and the parents, respectively.

788 We computed the matrix of Pearson and Spearman correlation coefficients with the R stats package
789 v4.3.2 (http://www.r-project.org/). We produced the violin plots using vioplot v0.4.0 (Adler *et al.*
790 2022), ggplot2 v3.4.3 (Wickham 2016) and reshape2 v1.4.4 (Wickham 2007) R packages. We
791 performed the principal component analysis (PCA) using the function *PCA* from the R base package,
792 assigning trait means to missing values. Plots were drawn using FactoMineR v2.8 (Lê *et al.* 2002),
793 factoextra v1.0.7 (Kassambara and Mundt 2020) and corrplot v0.92 (Wei and Simko 2021) packages.
794
795 **Phenotype heritability**

796 Because we could not perform replicated measurements of phenotypes for each strain for lipolysis,
797 proteolysis, growth rate and color, we only estimated the narrow sense heritability (h^2) of these
798 phenotypes across the five progenies by estimating the slope of linear regressions of the five F1
799 progenies mean trait values on the mean values of the parental pairs using the *lm* function from the R
800 base package. Extrolite production was determined for three crosses (SxN, RxN and RxL), with two
801 replicates for each strain; we therefore estimated broad-sense heritability (H^2) for these phenotypes for
802 each cross based on variability among replicates, in addition to narrow-sense heritability as for the
803 other phenotypes. Broad sense heritability was determined by performing a one-way ANOVA with the
804 *lm* function of the stats v4.2.1 package in R.

805 **Genotyping based on indels**

806 We genotyped 389 offspring from the cross RxN between LCP06136 (Roquefort; MAT1-1;
807 https://www.ebi.ac.uk/ SAMEA103939766) and LCP06133 (non-Roquefort; MAT1-2;
808 SAMEA103939763) with 200 markers with a polymorphism of amplification size between the two
809 parental strains, due to the presence of indels (Supplementary Table IND). Primers were designed (i)
810 to yield an amplicon size between 150 to 410 bp and a difference ranging from six to 20 bp between

alleles, (ii) to be compatible in multiplex and (iii) to be evenly distributed along the assembly of the reference genome available at the beginning of the study (FM164; EMBL accession numbers HG792015 to HG792062, Cheeseman & Ropars *et al.* 2014). Indels were detected after a whole assembly alignment (blast v2.9.0; Altschul *et al.* 1990) of the two parental strains with the gap and extension penalties set to 1. After adding 250 base pairs upstream and downstream from the hit position, we performed a multi-alignment using MAFFT (Katoh 2002) with the whole genomes of the parental strains of the other crosses. We only kept a consensus sequence generated using consambig (Rice et al. 2000) and designed primers using Primer3 (Untergasser *et al.* 2012).

To reduce the cost of fluorescence primers, we only used four universal fluorescent primers (M13(-21), D8S1132f, D12S1090f, DYS437f), labeled with different fluorescent dyes (FAM, ATTO550, ATTO565, YAKIMA Yellow; Eurofins, Ebersberg, Germany). The specific primers attached during PCR to universal fluorescent primers thanks to a tail added to each specific primer matching an edge of the universal primers (Schuelke 2000; Missiaggia and Grattapaglia 2006). For each locus, the PCR amplification thus required three primers: the forward fluorescent universal primer, the forward specific primer with a 5' tail corresponding to the chosen universal primer and the regular specific reverse primer. The 200 markers were genotyped in 25 multiplex groups of 8 locus organized according to their amplicon size and their color fluorescent dye (Supplementary Table 8). For each multiplex, two separate sets of quadruplex PCR reactions were performed to minimize the interaction between primers and then pooled into octoplexes for the genotyping step. The PCR mix contained 0.16 µM of each of the fluorescent universal primer and of the reverse specified primer and 0.04 µM of the 5' tail forward primer in a final 15 µl reaction volume (2x QIAGEN Multiplex PCR Master Mix with 3 mM Mg^{2+}, 10x primer mix with 1.6 or 0.4 µM of each primer, 3 µl of DNA diluted 50 fold) using the same PCR cycle conditions as for the microsatellites loci previously described in the recombinant offspring detection paragraph, except that it started with a hybridization temperature of 62°C instead of 60°C. Genotyping and analysis were also done as previously described in the recombinant offspring detection paragraph.

Genotyping based on GBS

For all five crosses, we genotyped the obtained progeny (1073 offspring in total) at the AGAP CIRAD platform with genotyping-by-sequencing using the *Ape*KI enzyme. DNAs were purified after digestion on QIAquick columns (Qiagen, Les Ulis, France) and their qualities were controlled using a TapeStation instrument (Agilent Technologies, Les Ulis, France). Sequencing was performed on an Illumina Hiseq 4000 (2x150 bp). The following numbers of recombinant offspring were genotyped by GBS: 384 for the cross RxN, 157 for the cross RxS, 185 for the cross RxL, 176 for the cross SxN and 171 for the cross LxN.

Demultiplexed reads were mapped to the LCP06136 high-quality genome for the crosses RxL and RxS and to the LCP06133 high-quality genome for the crosses RxN, LxN and SxN using *Bowtie2* version 2.3.4.1 (Langmead and Salzberg 2012; Langmead *et al.* 2019). In *Bowtie2,* we set the maximum length (-X) to 1000 and used the preset "very-sensitive-local". We used SAMtools v1.7 (Danecek *et al.* 2021) to sort and filter out duplicate reads and reads with a mapping quality score above ten for SNP calling. Single nucleotide polymorphisms (SNPs) were called using the GATK v4.1.2.0 Haplotype Caller (McKenna *et al.* 2010), generating a gVCF file per strain with option ploidy 2 to detect potential duplicated regions in progenies, as we had found indels with two alleles in some offspring. GVCFs were combined using GATK CombineGVCFs, genotypes with GATK GenotypeGVCFs, and biallelic SNPs were selected after filtration using GATK SelectVariants. We filtered SNPs using GATK VariantFiltration and options QUAL <30, DP < 5, QD < 20.0, FS > 60.0, MQ < 40, 0.05<AF<0.95, SOR > 3.0, MQRankSum < -12.5, ReadPosRankSum < -8.0, DP>5.0 and GQ<10. We generated the genotype matrix based on the VCF file with *Bcftools* v1.11 (Li 2011; Danecek *et al.* 2021). Markers with no data or with no differences between the two parental genomes were filtered out. To reconstruct offspring genotypes, we performed SNP calling in the diploid mode in order to detect double copies of translocated regions. Markers corresponding to the translocated regions were in fact called as heterozygous in some offspring; they were therefore placed in offspring at the two parental locations, which were each assigned the corresponding parental allele.

After performing crosses and isolating ascospores, we detected sectors of two slightly different morphotypes in subsequent cultures of the parental strain LCP06039 aiming at phenotype

865 measurements. However, genetic data indicated that the cross was performed with a pure strain and
866 not a mixture: (i) the indel genotypes of the two morphotypes were assessed and were identical, and
867 (ii) the GBS genotypes of the two morphotypes were not typed directly, but we did not detect genome-
868 wide segregation distortion in the progeny in GBS data for this cross, while a cross involving a
869 mixture of strains with different genotypes should result in over-representation of the alleles by the
870 pure parent; on the contrary, the segregation distortions detected in some genomic regions
871 corresponded to over-representations of the strain showing two morphotypes rather than its under-
872 representation. We therefore considered that a single strain contributed to the cross and that the two
873 morphotypes were the result of plasticity or a few somatic mutations in a single strain. We therefore
874 built the genetic map and ran a QTL analysis for the LxN cross. For analyses involving parental traits,
875 and therefore potentially affected by the presence of two morphotypes (*i.e.* for heritability estimates
876 and transgression detection) we computed estimates using all three possible values for the LCP06039
877 parent strain phenotype: the means of the trait values for the two morphotypes or the value of one of
878 the two morphotypes. This did not affect conclusions as the two morphotypes were actually very close
879 for all trait measures.

880 **Experiment on the stability of genotypes across replication**

881 As we identified a genomic region with two alleles present in multiple offspring in the RxN cross with
882 associated QTLs, we wanted to check whether this particular genotype was stable during strain culture
883 and across multiple replication steps. We therefore cultivated, on malt agar, the two parental strains
884 from the RxN cross and the 11 offspring for which genomes were sequenced with Nanopore, six with
885 alleles of both parents for this genomic region, four with the LCP06136 parental allele and one with
886 the LCP06133 allele. We cultivated the strains for one week on malt agar and replated them on a new
887 plate by transplanting some conidia from the edge of the colonies. We performed 19 replication steps.
888 In the end, we re-genotyped the lines with the six indel markers present in the rearranged region.

889 **Linkage map and QTL detection**

Obtained offpring phenotypes are presented in Supplementary Table 9 and offpring genotype are presented in Suplementary Tables 10, 11, 12, 13 and 14 for SxN, LxN, RxN, RxS and RxL crosses respectively. The genetic map and statistical tests for QTL association were performed using the R software v3.5.1 (http://www.r-project.org/) with the ASMap v1.0-5 package (Taylor and Butler 2017) for the genetic map and qtl v1.60 package (Broman *et al.* 2003) for statistical tests. For the genetic map, we used unique segregating markers with less than 10% missing data and markers with segregation distortion with significant Chi Square p-values adjusted with Bonferroni corrections. Individuals with more than 30% of missing data were filtered out (Table 1), concerning up to 14% of the offspring of a cross. Linkage groups and marker ordering were determined with the *mstmap* function of AsMap package, with parameter "bychr" set as FALSE and a p.value of 10^{-12}. Markers with less than 20% missing data and less than 95% of one parental allele were then reintegrated in linkage groups with the *pull.cross* function with "max.rf" and "min.lod" parameters set at 0.1 and 20, respectively. We reconstructed marker order in linkage groups with the *mstmap* function, the parameter "bychr" set as TRUE, and a p.value< 10^{-12}. We estimated genetic distances between markers with the AsMap *quickEst* function and the Kosambi's mapping function. We compared the obtained order to the reference genome order using the *compareorder* function of the qtl package with error probability set at 0.005. We changed the order only if it improved the LOD score and minimized the linkage group length. We represented the relationships between chromosome physical positions and genetic maps using ALLMAPS in JCVI utility libraries v1.3.6 (Tang *et al.* 2015), adapted to include genetic features.

We performed single QTL detection using the *scanone* function of the qtl package v1.6 with the threshold at 5% being estimated with 1000 permutations. We used the *addqtl* function of the qtl package to mask the first set of QTLs and thus detect additional QTLs that may have been hidden by the main ones. We estimated confidence intervals for QTL using the *lodint* function of the qtl package with default parameters. We identified QTL interactions using the *scantwo* function with the Haley-Knott method using a threshold at 5% estimated by 1,000 permutations. We performed analyses of variance (ANOVAs) using a linear model with the *fitqtl* function of the qtl package, keeping

interactions between loci only when they were significant in both *scantwo* and the full model AVOVAs. We extended QTL confidence intervals including the first or last marker of a linkage group to the start or end of the corresponding chromosome. For comparisons of QTL interval positions between crosses, we transposed the intervals determined with the positions on the Roquefort parent genomes (for RxL and RxS crosses) onto the non-Roquefort genome. To do this, we extracted genome sequences using bedtools getfasta v2.30.0 (Quinlan and Hall 2010) and mapped the extracted sequences onto the non-Roquefort parent genome using minimap2 v2.17-r941 (Li 2018). The representation of the aligned QTL intervals was constructed using the karyoplotR v1.24.0 package (Gel and Serra 2017).

Acknowledgements: This study has been funded by the ANR-19-CE20-0002-02 Fungadapt ANR, ERC Genomefun 309403 Stg, ERC Blue Proof of Concept, Fondation Louis D (French Academy of Sciences) grants, the LIP SAS and the ANRT (Association Nationale Recherche Technologie). TC and ECr acknowledge the E3GP3 network for facilitating collaborations and skills transfer from MF laboratory. We acknowledge the staff at the GENTYANE genotyping platform (INRAe GDEC, Clermont-Ferrand, France) for microsatellite and indel genotyping and the AGAP CIRAD platform for GBS sequencing. We gratefully acknowledge Intersciences for the loan and set-up of the ScanStation (https://www.interscience.com/en/products/real-time-incubator-and-colony-counter/). We thank Jeanne Ropars for her help in obtaining the progeny and Jean-Philippe Vernadet for help with bioinformatic analyses.

Author contribution

TG, TC, AB, DR, CC and MP designed the study. TG, DR, ECo and MP acquired funding. TC, AS and SLP performed crosses, isolated strains and extracted DNAs, supervised by TG. TC, MLP and SB performed experiments for phenotyping lipolysis, proteolysis and growth rates supervised by CC, DR and MP. TC, ASn and SLP performed genotyping and genome sequencing, supervised by TG. ECr and GC performed experiments for estimating the production of extrolites supervised by MC. TC and ASn performed the experiment on the stability of genotypes across replication and the Oxford

Nanopore sequencing, supervised by TG. TC, ECr, ASi and RRdlV performed the genomic analyses, supervised by TG, MFO and AB. TC, TG and ECr wrote the manuscript. All authors revised the manuscript.

Data availability

All accession numbers will be available upon manuscript acceptance.

References

Adamczyk, K., Pokorska, J., Makulska, J., Earley, B., & Mazurek, M. (2013). Genetic analysis and evaluation of behavioural traits in cattle. *Livestock Science*, *154*, 1–12. https://doi.org/10.1016/j.livsci.2013.01.016

Adler, D., Kelly, T., Elliott, T., & Adamson, J. (2022). *vioplot: Violin plot.* (0.4.0) [Computer software]. https://github.com/TomKellyGenetics/vioplot

Alexa, A., & Rahnenfuhrer, J. (2016). *topGO: Enrichment Analysis for Gene Ontology* [Computer software]. https://bioconductor.org/packages/release/bioc/html/topGO.html

Alonge, M., Lebeigle, L., Kirsche, M., Jenike, K., Ou, S., Aganezov, S., Wang, X., Lippman, Z. B., Schatz, M. C., & Soyk, S. (2022). Automated assembly scaffolding using RagTag elevates a new tomato system for high-throughput genome editing. *Genome Biology*, *23*(1), 258. https://doi.org/10.1186/s13059-022-02823-7

Altschul, S. F., Gish, W., Miller, W., Myers, E. W., & Lipman, D. J. (1990). Basic Local Alignment Search Tool. *Journal of Molecular Biology*, *215*(3), 403–410. https://doi.org/10.1016/S0022-2836(05)80360-2

Andargie, M., Pasquet, R. S., Gowda, B. S., Muluvi, G. M., & Timko, M. P. (2014). Molecular mapping of QTLs for domestication-related traits in cowpea (*V. unguiculata* (L.) Walp.). *Euphytica*, *200*(3), 401–412. https://doi.org/10.1007/s10681-014-1170-9

967 Baack, E. J., Sapir, Y., Chapman, M. A., Burke, J. M., & Rieseberg, L. H. (2008). Selection on
968 domestication traits and quantitative trait loci in crop–wild sunflower hybrids. *Molecular Ecology*,
969 *17*(2), 666–677. https://doi.org/10.1111/j.1365-294X.2007.03596.x

970 Bachlava, E., Tang, S., Pizarro, G., Schuppert, G. F., Brunick, R. K., Draeger, D., Leon, A., Hahn, V.,
971 & Knapp, S. J. (2010). Pleiotropy of the branching locus (*B*) masks linked and unlinked quantitative
972 trait loci affecting seed traits in sunflower. *Theoretical and Applied Genetics*, *120*(4), 829–842.
973 https://doi.org/10.1007/s00122-009-1212-1

974 Bernardes, J. P., Stelkens, R. B., & Greig, D. (2017). Heterosis in hybrids within and between yeast
975 species. *Journal of Evolutionary Biology*, *30*(3), 538–548. https://doi.org/10.1111/jeb.13023

976 Böhm, J., Hoff, B., O'Gorman, C. M., Wolfers, S., Klix, V., Binger, D., Zadra, I., Pöggeler, S., Dyer,
977 P. S., & Kück, U. (2012). Sexual reproduction and mating-type – mediated strain development in the
978 penicillin-producing fungus *Penicillium chrysogenum*. *Proceedings of the National Academy of*
979 *Sciences*, *110*(4), 1476–1481. https://doi.org/10.1073/pnas.1217943110/-
980 /DCSupplemental.www.pnas.org/cgi/doi/10.1073/pnas.1217943110

981 Bolger, A. M., Lohse, M., & Usadel, B. (2014). Trimmomatic: A flexible trimmer for Illumina
982 sequence data. *Bioinformatics*, *30*(15), 2114–2120. https://doi.org/10.1093/bioinformatics/btu170

983 Bomblies, K., & Doebley, J. F. (2006). Pleiotropic effects of the duplicate maize
984 *FLORICAULA/LEAFY* genes *zfl1* and *zfl2* on traits under selection during maize domestication.
985 *Genetics*, *172*(1), 519–531. https://doi.org/10.1534/genetics.105.048595

986 Broman, K. W., Wu, H., Sen, Ś., & Churchill, G. A. (2003). R/qtl: QTL mapping in experimental
987 crosses. *Bioinformatics*, *19*(7), 889–890. https://doi.org/10.1093/bioinformatics/btg112

988 Brůna, T., Lomsadze, A., & Borodovsky, M. (2020). GeneMark-EP+: Eukaryotic gene prediction with
989 self-training in the space of genes and proteins. NAR Genomics and Bioinformatics, 2(2), lqaa026.
990 https://doi.org/10.1093/nargab/lqaa026

991 Brůna, T., Hoff, K. J., Lomsadze, A., Stanke, M., & Borodovsky, M. (2021). BRAKER2: Automatic
992 eukaryotic genome annotation with GeneMark-EP+ and AUGUSTUS supported by a protein database.
993 *NAR Genomics and Bioinformatics*, *3*(1), lqaa108. https://doi.org/10.1093/nargab/lqaa108

994 Buchanan, R. L., Golden, M. H., & Whiting, R. C. (1993). Differentiation of the effects of pH and
995 lactic or acetic acid concentration on the kinetics of *Listeria monocytogenes* inactivation. *Journal of*
996 *Food Protection*, *56*(6), 474–479. https://doi.org/10.4315/0362-028X-56.6.474

997 Buchfink, B., Xie, C., & Huson, D. H. (2015). Fast and sensitive protein alignment using DIAMOND.
998 Nature Methods, 12(1), 59–60. https://doi.org/10.1038/nmeth.3176

999 Bucknell, A. H., & McDonald, M. C. (2023). That's no moon, it's a *Starship*: Giant transposons
1000 driving fungal horizontal gene transfer. *Molecular Microbiology*, mmi.15118.
1001 https://doi.org/10.1111/mmi.15118

1002 Camacho, C., Coulouris, G., Avagyan, V., Ma, N., Papadopoulos, J., Bealer, K., & Madden, T. L.
1003 (2009). BLAST+: Architecture and applications. BMC Bioinformatics, 10(1), 421.
1004 https://doi.org/10.1186/1471-2105-10-421

1005 Cantor, M. D., Van Den Tempel, T., Hansen, T. K., & Ardö, Y. (2004). Blue cheese. *Cheese:*
1006 *Chemistry, Physics and Microbiology*, *2*, 175–198. https://doi.org/10.1016/S1874-558X(04)80044-7

1007 Caron, T., Piver, M. L., Péron, A.-C., Lieben, P., Lavigne, R., Brunel, S., Roueyre, D., Place, M.,
1008 Bonnarme, P., Giraud, T., Branca, A., Landaud, S., & Chassard, C. (2021). Strong effect of
1009 *Penicillium roqueforti* populations on volatile and metabolic compounds responsible for aromas,
1010 flavor and texture in blue cheeses. *International Journal of Food Microbiology*, *354*, 109174.
1011 https://doi.org/10.1016/j.ijfoodmicro.2021.109174

1012 Cerning, J., Gripon, J.-C., Lamberet, G., & Lenoir, J. (1987). Les activités biochimiques des
1013 *Penicillium* utilisés en fromagerie. *Le Lait*, *67*(1), 3–39. https://doi.org/10.1051/lait:198711

1014 Chávez, R., Vaca, I., & García-Estrada, C. (2023). Secondary metabolites produced by the blue-cheese
1015 ripening mold *Penicillium roqueforti*; biosynthesis and regulation mechanisms. *Journal of Fungi*, *9*(4),
1016 459. https://doi.org/10.3390/jof9040459

1017 Cheeseman, K., Ropars, J., Renault, P., Dupont, J., Gouzy, J., Branca, A., Abraham, A.-L., Ceppi, M.,
1018 Conseiller, E., Bensimon, A., Giraud, T., & Brygoo, Y. (2014). Multiple recent horizontal transfers of
1019 a large genomic region in cheese making fungi. *Nature Communications*, *5*, 2876.
1020 https://doi.org/10.1038/ncomms3876

1021 Cleere, M. M., Novodvorska, M., Geib, E., Whittaker, J., Dalton, H., Salih, N., Hewitt, S., Kokolski,
1022 M., Brock, M., & Dyer, P. S. (2024). New colors for old in the blue-cheese fungus Penicillium
1023 roqueforti. Npj Science of Food, 8(1), 3. https://doi.org/10.1038/s41538-023-00244-9

1024 Collins, Y. F., McSweeney, P. L. H., & Wilkinson, M. G. (2003). Lipolysis and free fatty acid
1025 catabolism in cheese: A review of current knowledge. *International Dairy Journal*, *13*(11), 841–866.
1026 https://doi.org/10.1016/S0958-6946(03)00109-2

1027 Coluccio, A., Bogengruber, E., Conrad, M. N., Dresser, M. E., Briza, P., & Neiman, A. M. (2004).
1028 Morphogenetic pathway of spore wall assembly in *Saccharomyces cerevisiae*. *Eukaryotic Cell*, *3*(6),
1029 1464–1475. https://doi.org/10.1128/EC.3.6.1464-1475.2004

1030 Conrado, R., Gomes, T. C., Roque, G. S. C., & De Souza, A. O. (2022). Overview of bioactive fungal
1031 secondary metabolites: Cytotoxic and antimicrobial compounds. *Antibiotics*, *11*(11), 1604.
1032 https://doi.org/10.3390/antibiotics11111604

1033 Cosciani-Cunico, E., Dalzini, E., Ducoli, S., Sfameni, C., Bertasi, B., Losio, M.-N., Daminelli, P., &
1034 Varisco, G. (2015). Behaviour of *Listeria monocytogenes* and *Escherichia coli* O157:H7 during the
1035 cheese making of traditional raw-milk cheeses from Italian Alps. *Italian Journal of Food Safety*, *4*(2).
1036 https://doi.org/10.4081/ijfs.2015.4585

1037 Coton, E., Coton, M., Hymery, N., Jany, J. L., & Mounier, J. (2020). *Penicillium roqueforti*: An
1038 overview of its genetics, physiology, metabolism and biotechnological applications. *Fungal Biology*
1039 *Reviews*, *34*(2), 59–73. https://doi.org/10.1016/j.fbr.2020.03.001

1040 Crequer, E., Ropars, J., Jany, L., Caron, T., Coton, M., Snirc, A., Vernadet, P., Branca, A., Giraud, T.,
1041 & Coton, E. (2023). A new cheese population in Penicillium roqueforti and adaptation of the five
1042 populations to their ecological niche. Evolutionary Applications, 1–20.
1043 https://doi.org/10.1111/eva.13578

1044 Crequer, E., Coton, E., Cueff, G., Cristiansen, J. V., Frisvad, J. C., De La Vega, R. R., Giraud, T.,
1045 Jany, J.-L., & Coton, M. (2024). Different metabolite profiles across Penicillium roqueforti
1046 populations associated with ecological niche specialisation and domestication [Preprint].
1047 Microbiology. https://doi.org/10.1101/2024.01.12.575369

1048 Cryer, N. C., Butler, D. R., & Wilkinson, M. J. (2005). High throughput, high resolution selection of
1049 polymorphic microsatellite loci for multiplex analysis. *Plant Methods*, *1*, 1–5.
1050 https://doi.org/10.1186/1746-4811-1-3

1051 Danecek, P., Bonfield, J. K., Liddle, J., Marshall, J., Ohan, V., Pollard, M. O., Whitwham, A., Keane,
1052 T., McCarthy, S. A., Davies, R. M., & Li, H. (2021). Twelve years of SAMtools and BCFtools.
1053 *GigaScience*, *10*(2), giab008. https://doi.org/10.1093/gigascience/giab008

1054 Dobin, A., Davis, C. A., Schlesinger, F., Drenkow, J., Zaleski, C., Jha, S., Batut, P., Chaisson, M., &
1055 Gingeras, T. R. (2013). STAR: Ultrafast universal RNA-seq aligner. *Bioinformatics*, *29*(1), 15–21.
1056 https://doi.org/10.1093/bioinformatics/bts635

1057 Doebley, J., Stec, A., & Hubbard, L. (1997). The evolution of apical dominance in maize. *Nature*,
1058 *386*(6624), 485–488. https://doi.org/10.1038/386485a0

1059 Dumas, É., Feurtey, A., Rodríguez de la Vega, R. C., Le Prieur, S., Snirc, A., Coton, M., Thierry, A.,
1060 Coton, E., Le Piver, M., Roueyre, D., Ropars, J., Branca, A., & Giraud, T. (2020). Independent

1061 domestication events in the blue-cheese fungus *Penicillium roqueforti*. *Molecular Ecology*,
1062 *33913*(January), 451773. https://doi.org/10.1111/mec.15359

1063 Eder, M., Sanchez, I., Brice, C., Camarasa, C., Legras, J.-L., & Dequin, S. (2018). Qtl mapping of
1064 volatile compound production in *Saccharomyces cerevisiae* during alcoholic fermentation. *BMC*
1065 *Genomics*, *19*, 166. https://doi.org/10.1186/s12864-018-4562-8

1066 Enyenihi, A. H., & Saunders, W. S. (2003). Large-Scale Functional Genomic Analysis of Sporulation
1067 and Meiosis in *Saccharomyces cerevisiae*. *Genetics*, *163*(1), 47–54.
1068 https://doi.org/10.1093/genetics/163.1.47

1069 Fairclough, A. C., Cliffe, D. E., & Knapper, S. (2011). Factors affecting *Penicillium roquefortii*
1070 (*Penicillium glaucum*) in internally mould ripened cheeses: Implications for pre-packed blue cheeses.
1071 *International Journal of Food Science & Technology*, *46*, 1586–1590. https://doi.org/10.1111/j.1365-
1072 2621.2011.02658.x

1073 Falconer, D. S., & Mackay, T. F. C. (1995). *Introduction to Quantitative Genetics*. Pearson Education
1074 Limited.

1075 Flutre, T., Duprat, E., Feuillet, C., & Quesneville, H. (2011). Considering Transposable Element
1076 Diversification in *De Novo* Annotation Approaches. *PLoS ONE*, *6*(1), e16526.
1077 https://doi.org/10.1371/journal.pone.0016526

1078 Fontaine, K., Hymery, N., Lacroix, M. Z., Puel, S., Puel, O., Rigalma, K., Gaydou, V., Coton, E., &
1079 Mounier, J. (2015). Influence of intraspecific variability and abiotic factors on mycotoxin production
1080 in *Penicillium roqueforti*. *International Journal of Food Microbiology*, *215*, 187–193.
1081 https://doi.org/10.1016/j.ijfoodmicro.2015.07.021

1082 Foulongne-Oriol, M., Rodier, A., Rousseau, T., & Savoie, J.-M. (2012). Quantitative trait locus
1083 mapping of yield-related components and oligogenic control of the cap color of the button mushroom,

1084 *Agaricus bisporus*. *Applied and Environmental Microbiology*, *78*(7), 2422–2434.
1085 https://doi.org/10.1128/AEM.07516-11

1086 Fox, J., & Weisberg, S. (2019). *An {R} Companion to applied regression* (T. Oaks, Ed.). Sage.
1087 https://socialsciences.mcmaster.ca/jfox/Books/Companion/

1088 Frisvad, J. C., & Filtenborg, O. (1983). Classification of terverticillate *Penicillia* based on profiles of
1089 mycotoxins and other secondary metabolites. Applied and Environmental Microbiology, 46(6), 1301–
1090 1310. https://doi.org/10.1128/aem.46.6.1301-1310.1983

1091 Galagan, J. E., & Selker, E. U. (2004). RIP: The evolutionary cost of genome defense. *Trends in*
1092 *Genetics*, *20*(9), 417–423. https://doi.org/10.1016/j.tig.2004.07.007

1093 Galloway, L. D., & Burgess, R. (1952). Galloway L.D. and Burgess R.(1952) Applied Mycology and
1094 Bacteriology 3rd Edition Leonard Hill, London. Pp54 and 57. Applied Mycology and Bacteriology, 3,
1095 54–57.

1096 Ge, H. M., Yu, Z. G., Zhang, J., Wu, J. H., & Tan, R. X. (2009). Bioactive alkaloids from endophytic
1097 *Aspergillus fumigatus*. *Journal of Natural Products*, *72*(4), 753–755.
1098 https://doi.org/10.1021/np800700e

1099 Gel, B., & Serra, E. (2017). karyoploteR: An R/Bioconductor package to plot customizable genomes
1100 displaying arbitrary data. *Bioinformatics*, *33*(19), 3088–3090.
1101 https://doi.org/10.1093/bioinformatics/btx346

1102 Gil-Durán, C., Rojas-Aedo, J. F., Medina, E., Vaca, I., García-Rico, R. O., Villagrán, S., Levicán, G.,
1103 & Chávez, R. (2015). The *pcz1* gene, which encodes a Zn(II)2Cys6 Protein, is involved in the control
1104 of growth, conidiation, and conidial germination in the filamentous fungus *Penicillium roqueforti*.
1105 *PLOS ONE*, *10*(3), e0120740. https://doi.org/10.1371/journal.pone.0120740

1106 Gillot, G., Jany, J.-L., Coton, M., Le Floch, G., Debaets, S., Ropars, J., López-Villavicencio, M.,
1107 Dupont, J., Branca, A., Giraud, T., & Coton, E. (2015). (Fifty shades of blue□:) Insights into

Penicillium roqueforti morphological and genetic diversity. PLoS ONE, 10(6), e0129849. https://doi.org/10.1371/journal.pone.0129849

Gillot, G., Jany, J.-L., Poirier, E., Maillard, M., Debaets, S., Thierry, A., Coton, E., & Coton, M. (2017). Functional diversity within the *Penicillium roqueforti* species. *International Journal of Food Microbiology*, *241*, 141–150. https://doi.org/10.1016/j.ijfoodmicro.2016.10.001

Gladieux, P., Ropars, J., Badouin, H., Branca, A., Aguileta, G., De Vienne, D. M., Rodríguez de la Vega, R. C., Branco, S., & Giraud, T. (2014). Fungal evolutionary genomics provides insight into the mechanisms of adaptive divergence in eukaryotes. *Molecular Ecology*, *23*(4), 753–773. https://doi.org/10.1111/mec.12631

Gluck-Thaler, E., Ralston, T., Konkel, Z., Ocampos, C. G., Ganeshan, V. D., Dorrance, A. E., Niblack, T. L., Wood, C. W., Slot, J. C., Lopez-Nicora, H. D., & Vogan, A. A. (2022). Giant *Starship* elements mobilize accessory genes in fungal genomes. *Molecular Biology and Evolution*, *39*(5), msac109. https://doi.org/10.1093/molbev/msac109

Gotoh, O., Morita, M., & Nelson, D. R. (2014). Assessment and refinement of eukaryotic gene structure prediction with gene-structure-aware multiple protein sequence alignment. BMC Bioinformatics, 15(1), 189. https://doi.org/10.1186/1471-2105-15-189

Grognet, P., Lalucque, H., Malagnac, F., & Silar, P. (2014). Genes that bias mendelian segregation. *PLoS Genetics*, *10*(5), e1004387. https://doi.org/10.1371/journal.pgen.1004387

Gurevich, A., Saveliev, V., Vyahhi, N., & Tesler, G. (2013). QUAST: Quality assessment tool for genome assemblies. *Bioinformatics*, *29*(8), 1072–1075. https://doi.org/10.1093/bioinformatics/btt086

Hall, B., Hall, M., Statisticat, L., Brown, E., Hermanson, R., Charpentier, E., Heckq, D., Laurent, S., Gronau, Q. F., & Singmann, H. (2021). *Package "LaplacesDemon"* (16.1.6) [Computer software]. https://github.com/LaplacesDemonR/LaplacesDemon

1131 Hoede, C., Arnoux, S., Moisset, M., Chaumier, T., Inizan, O., Jamilloux, V., & Quesneville, H.
1132 (2014). PASTEC: An Automatic transposable element classification tool. *PLoS ONE*, *9*(5), e91929.
1133 https://doi.org/10.1371/journal.pone.0091929

1134 Hoff, K. J., Lange, S., Lomsadze, A., Borodovsky, M., & Stanke, M. (2016). BRAKER1:
1135 Unsupervised RNA-Seq-Based Genome Annotation with GeneMark-ET and AUGUSTUS.
1136 Bioinformatics, 32(5), 767–769. https://doi.org/10.1093/bioinformatics/btv661

1137 Hoff, K. J., Lomsadze, A., Borodovsky, M., & Stanke, M. (2019). Whole-Genome Annotation with
1138 BRAKER. Gene Prediction, 1962, 65–95. https://doi.org/10.1007/978-1-4939-9173-0_5

1139 Hymery, N., Puel, O., Tadrist, S., Canlet, C., Le Scouarnec, H., Coton, E., & Coton, M. (2017). Effect
1140 of PR toxin on THP1 and Caco-2 cells: An *in vitro* study. *World Mycotoxin Journal*, *10*(4), 375–386.
1141 https://doi.org/10.3920/WMJ2017.2196

1142 Imbernon, M., Callac, P., Gasqui, P., Kerrigan, R. W., & Velcko, A. J. (1996). *BSN*, the primary
1143 determinant of basidial spore number and reproductive mode in *Agaricus bisporus*, maps to
1144 chromosome *I*. *Mycologia*, *88*(5), 749–761. https://doi.org/10.1080/00275514.1996.12026713

1145 Iwata, H., & Gotoh, O. (2012). Benchmarking spliced alignment programs including Spaln2, an
1146 extended version of Spaln that incorporates additional species-specific features. Nucleic Acids
1147 Research, 40(20), e161–e161. https://doi.org/10.1093/nar/gks708

1148 Jadhav, M. S. (2015). An update on important functionally characterized genes / QTLs of agronomic
1149 importance in crop plants. *Indian Research Journal of Genetics & Biotechnology*, *7*(1), 44–49.

1150 Jakubczyk, K., Kałduńska, J., Kochman, J., & Janda, K. (2020). Chemical Profile and Antioxidant
1151 Activity of the Kombucha Beverage Derived from White, Green, Black and Red Tea. *Antioxidants*,
1152 *9*(5), 447. https://doi.org/10.3390/antiox9050447

1153 Johnsson, M., Rubin, C. J., Höglund, A., Sahlqvist, A. S., Jonsson, K. B., Kerje, S., Ekwall, O.,
1154 Kämpe, O., Andersson, L., Jensen, P., & Wright, D. (2014). The role of pleiotropy and linkage in

genes affecting a sexual ornament and bone allocation in the chicken. *Molecular Ecology*, *23*(9), 2275–2286. https://doi.org/10.1111/mec.12723

Kantar, M. B., Nashoba, A. R., Anderson, J. E., Blackman, B. K., & Rieseberg, L. H. (2017). The Genetics and Genomics of Plant Domestication. *BioScience*, *67*(11), 971–982. https://doi.org/10.1093/biosci/bix114

Kassambara, A., & Mundt, F. (2020). *factoextra: Extract and Visualize the Results of Multivariate Data Analyses* (R package version 1.0.7) [Computer software]. https://CRAN.R-project.org/package=factoextra

Katoh, K. (2002). MAFFT: a novel method for rapid multiple sequence alignment based on fast Fourier transform. *Nucleic Acids Research*, *30*(14), 3059–3066. https://doi.org/10.1093/nar/gkf436

Kessi-Pérez, E. I., Molinet, J., & Martínez, C. (2020). Disentangling the genetic bases of *Saccharomyces cerevisiae* nitrogen consumption and adaptation to low nitrogen environments in wine fermentation. *Biological Research*, *53*(1), 1–10. https://doi.org/10.1186/s40659-019-0270-3

Kieslich, P. J., Henninger, F., Wulff, D. U., Haslbeck, J. M. B., & Schulte-Mecklenbeck, M. (2019). Mouse-tracking: A practical guide to implementation and analysis. In *A handbook of process tracing methods*. PsyArXiv. https://doi.org/10.31234/osf.io/zuvqa

Kolmogorov, M., Armstrong, J., Raney, B. J., Streeter, I., Dunn, M., Yang, F., Odom, D., Flicek, P., Keane, T. M., Thybert, D., Paten, B., & Pham, S. (2018). Chromosome assembly of large and complex genomes using multiple references. *Genome Research*, *28*(11), 1720–1732. https://doi.org/10.1101/gr.236273.118

Kolmogorov, M., Yuan, J., Lin, Y., & Pevzner, P. A. (2019). Assembly of long, error-prone reads using repeat graphs. *Nature Biotechnology*, *37*(5), 540–546. https://doi.org/10.1038/s41587-019-0072-8

1178 Kongjaimun, A., Kaga, A., Tomooka, N., Somta, P., Vaughan, D. A., & Srinives, P. (2012). The
1179 genetics of domestication of yardlong bean, *Vigna unguiculata* (L.) Walp. Ssp. *Unguiculata* cv.-gr.
1180 *Sesquipedalis*. *Annals of Botany*, *109*(6), 1185–1200. https://doi.org/10.1093/aob/mcs048

1181 Koren, S., Walenz, B. P., Berlin, K., Miller, J. R., Bergman, N. H., & Phillippy, A. M. (2017). Canu:
1182 Scalable and accurate long-read assembly via adaptive *k* -mer weighting and repeat separation.
1183 *Genome Research*, *27*(5), 722–736. https://doi.org/10.1101/gr.215087.116

1184 Krzywinski, M., Schein, J., Birol, İ., Connors, J., Gascoyne, R., Horsman, D., Jones, S. J., & Marra,
1185 M. A. (2009). Circos: An information aesthetic for comparative genomics. *Genome Research*, *19*(9),
1186 1639–1645. https://doi.org/10.1101/gr.092759.109

1187 Kumar, J., Gupta, D. S., Gupta, S., Dubey, S., Gupta, P., & Kumar, S. (2017). Quantitative trait loci
1188 from identification to exploitation for crop improvement. *Plant Cell Reports*, *36*(8), 1187–1213.
1189 https://doi.org/10.1007/s00299-017-2127-y

1190 Kurtz, S., Phillippy, A., Delcher, A. L., Smoot, M., Shumway, M., Antonescu, C., & Salzberg, S. L.
1191 (2004). Versatile and open software for comparing large genomes. *Genome Biology*, *5*, R12.
1192 https://doi.org/10.1186/gb-2004-5-2-r12

1193 Langmead, B., & Salzberg, S. L. (2012). Fast gapped-read alignment with Bowtie 2. *Nature Methods*,
1194 *9*(4), 357–359. https://doi.org/10.1038/nmeth.1923

1195 Langmead, B., Wilks, C., Antonescu, V., & Charles, R. (2019). Scaling read aligners to hundreds of
1196 threads on general-purpose processors. *Bioinformatics*, *35*(3), 421–432.
1197 https://doi.org/10.1093/bioinformatics/bty648

1198 Laurent, B., Moinard, M., Spataro, C., Chéreau, S., Zehraoui, E., Blanc, R., Lasserre, P., Ponts, N., &
1199 Foulongne-Oriol, M. (2021). QTL mapping in *Fusarium graminearum* identified an allele of FgVe1
1200 involved in reduced aggressiveness. *Fungal Genetics and Biology*, *153*, 103566.
1201 https://doi.org/10.1016/j.fgb.2021.103566

1202 Lê, S., Josse, J., & Husson, F. (2008). FactoMineR: An *R* Package for Multivariate Analysis. *Journal*
1203 *of Statistical Software*, *25*(1). https://doi.org/10.18637/jss.v025.i01

1204 Li, H. (2011). A statistical framework for SNP calling, mutation discovery, association mapping and
1205 population genetical parameter estimation from sequencing data. *Bioinformatics*, *27*(21), 2987–2993.
1206 https://doi.org/10.1093/bioinformatics/btr509

1207 Li, H. (2018). Minimap2: Pairwise alignment for nucleotide sequences. *Bioinformatics*, *34*(18), 3094–
1208 3100. https://doi.org/10.1093/bioinformatics/bty191

1209 Liti, G., & Louis, E. J. (2012). Advances in Quantitative Trait Analysis in Yeast. *PLoS Genetics*, *8*(8),
1210 e1002912. https://doi.org/10.1371/journal.pgen.1002912

1211 Lo, Y.-C., Bruxaux, J., Rodríguez de la Vega, R. C., Snirc, A., Coton, M., Piver, M. L., Prieur, S. L.,
1212 Roueyre, D., Dupont, J., Houbraken, J., Debuchy, R., Ropars, J., Giraud, T., & Branca, A. (2022).
1213 Domestication in dry-cured meat Penicillium fungi: Convergent specific phenotypes and horizontal
1214 gene transfers without strong genetic subdivision. https://doi.org/10.1101/2022.03.25.485132

1215 Lomsadze, A. (2005). Gene identification in novel eukaryotic genomes by self-training algorithm.
1216 Nucleic Acids Research, 33(20), 6494–6506. https://doi.org/10.1093/nar/gki937

1217 Lomsadze, A., Burns, P. D., & Borodovsky, M. (2014). Integration of mapped RNA-Seq reads into
1218 automatic training of eukaryotic gene finding algorithm. Nucleic Acids Research, 42(15), e119–e119.
1219 https://doi.org/10.1093/nar/gku557

1220 Luo, R., Liu, B., Xie, Y., Li, Z., Huang, W., Yuan, J., He, G., Chen, Y., Pan, Q., Liu, Y., Tang, J., Wu,
1221 G., Zhang, H., Shi, Y., Liu, Y., Yu, C., Wang, B., Lu, Y., Han, C., … Wang, J. (2012). SOAPdenovo2:
1222 An empirically improved memory-efficient short-read *de novo* assembler. *GigaScience*, *1*(1), 18.
1223 https://doi.org/10.1186/2047-217X-1-18

1224 Maechler, M. (2016). *Diptest: Hartigan's Dip Test Statistic for Unimodality—Corrected*.
1225 https://cran.r-project.org/package=diptest

1226 Manni, M., Berkeley, M. R., Seppey, M., Simão, F. A., & Zdobnov, E. M. (2021). BUSCO Update:
1227 Novel and Streamlined Workflows along with Broader and Deeper Phylogenetic Coverage for Scoring
1228 of Eukaryotic, Prokaryotic, and Viral Genomes. *Molecular Biology and Evolution*, *38*(10), 4647–4654.
1229 https://doi.org/10.1093/molbev/msab199

1230 Marcano, Y., Montanares, M., Gil-Durán, C., González, K., Levicán, G., Vaca, I., & Chávez, R.
1231 (2023). Pr*laeA* Affects the Production of Roquefortine C, Mycophenolic Acid, and Andrastin A in
1232 *Penicillium roqueforti*, but It Has Little Impact on Asexual Development. *Journal of Fungi*, *9*(10),
1233 954. https://doi.org/10.3390/jof9100954

1234 Marquina, M., Lambea, E., Carmona, M., Sánchez-Marinas, M., López-Aviles, S., Ayte, J., Hidalgo,
1235 E., & Aligue, R. (2022). A new negative feedback mechanism for MAPK pathway inactivation
1236 through Srk1 MAPKAP kinase. *Scientific Reports*, *12*(1), 19501. https://doi.org/10.1038/s41598-022-
1237 23970-8

1238 Martínez-Ainsworth, N. E., & Tenaillon, M. I. (2016). Superheroes and masterminds of plant
1239 domestication. *Comptes Rendus Biologies*, *339*(7–8), 268–273.
1240 https://doi.org/10.1016/j.crvi.2016.05.005

1241 Matas, A. J., Smith, J. M., Skeans, M. A., Thompson, B., Gustafson, S. K., Stewart, D. E., Cherikh, W.
1242 S., Wainright, J. L., Boyle, G., Snyder, J. J., Israni, A. K., & Kasiske, B. L. (2013). OPTN/SRTR 2013
1243 Annual Data Report: Kidney. *American Journal of Transplantation*, *15*, 1–34.
1244 https://doi.org/10.1111/ajt.13195

1245 Matsuda, Y., Awakawa, T., & Abe, I. (2013). Reconstituted biosynthesis of fungal meroterpenoid
1246 andrastin A. *Tetrahedron*, *69*(38), 8199–8204. https://doi.org/10.1016/j.tet.2013.07.029

1247 McKenna, A., Hanna, M., Banks, E., Sivachenko, A., Cibulskis, K., Kernytsky, A., Garimella, K.,
1248 Altshuler, D., Gabriel, S., Daly, M., & DePristo, M. A. (2010). The Genome Analysis Toolkit: A
1249 MapReduce framework for analyzing next-generation DNA sequencing data. *Genome Research*,
1250 *20*(9), 1297–1303. https://doi.org/10.1101/gr.107524.110

1251 Missiaggia, A., & Grattapaglia, D. (2006). Plant microsatellite genotyping with 4-color fluorescent
1252 detection using multiple-tailed primers. *Genetics and Molecular Research*, *5*(1), 72–78.

1253 Moreau, C. (1980). Le *Penicillium roqueforti*, morphologie, physiologie, intérêt en industrie
1254 fromagère, mycotoxines. *Le Lait*, *60*(595–596), 254–271. https://doi.org/10.1051/lait:1980595-59615

1255 Nguyen Ba, A. N., Lawrence, K. R., Rego-Costa, A., Gopalakrishnan, S., Temko, D., Michor, F., &
1256 Desai, M. M. (2022). Barcoded bulk QTL mapping reveals highly polygenic and epistatic architecture
1257 of complex traits in yeast. *eLife*, *11*, e73983. https://doi.org/10.7554/eLife.73983

1258 O'Gorman, C. M., Fuller, H. T., & Dyer, P. S. (2009). Discovery of a sexual cycle in the opportunistic
1259 fungal pathogen *Aspergillus fumigatus*. *Nature*, *457*, 471–475. https://doi.org/10.1038/nature07528

1260 Palmer, J., & Stajich, J. E. (2020). Funannotate v1.8.1: Eukaryotic genome annotation (1.8.1)
1261 [Computer software]. https://zenodo.org/record/4054262.

1262 Peltier, E., Bibi-Triki, S., Dutreux, F., Caradec, C., Friedrich, A., Llorente, B., & Schacherer, J.
1263 (2021). Dissection of quantitative trait loci in the *Lachancea waltii* yeast species highlights major
1264 hotspots. *G3 Genes|Genomes|Genetics*, *11*(9), jkab242. https://doi.org/10.1093/g3journal/jkab242

1265 Petrizzelli, M., De Vienne, D., & Dillmann, C. (2019). Decoupling the Variances of Heterosis and
1266 Inbreeding Effects Is Evidenced in Yeast's Life-History and Proteomic Traits. *Genetics*, *211*(2), 741–
1267 756. https://doi.org/10.1534/genetics.118.301635

1268 Pfister, R., Schwarz, K. A., Janczyk, M., Dale, R., & Freeman, J. B. (2013). Good things peak in pairs:
1269 A note on the bimodality coefficient. *Frontiers in Psychology*, *4*.
1270 https://doi.org/10.3389/fpsyg.2013.00700

1271 Pinheiro, J., Bates, D., DebRoy, S., Sarkar, D., & R Core Team. (2018). *{nlme}: Linear and Nonlinear*
1272 *Mixed Effects Models*. https://cran.r-project.org/package=nlme

1273 Punt, M., van den Brule, T., Teertstra, W. R., Dijksterhuis, J., den Besten, H. M. W., Ohm, R. A., &
1274 Wösten, H. A. B. (2020). Impact of maturation and growth temperature on cell-size distribution, heat-
1275 resistance, compatible solute composition and transcription profiles of *Penicillium roqueforti* conidia.
1276 *Food Research International*, *136*, 109287. https://doi.org/10.1016/j.foodres.2020.109287

1277 Quesneville, H., Bergman, C. M., Andrieu, O., Autard, D., Nouaud, D., Ashburner, M., &
1278 Anxolabehere, D. (2005). Combined Evidence Annotation of Transposable Elements in Genome
1279 Sequences. *PLoS Computational Biology*, *1*(2), e22. https://doi.org/10.1371/journal.pcbi.0010022

1280 Quinlan, A. R., & Hall, I. M. (2010). BEDTools: A flexible suite of utilities for comparing genomic
1281 features. *Bioinformatics*, *26*(6), 841–842. https://doi.org/10.1093/bioinformatics/btq033

1282 Rice, P., Longden, L., & Bleasby, A. (2000). EMBOSS: The European Molecular Biology Open
1283 Software Suite. *Trends in Genetics*, *16*(6), 276–277. https://doi.org/10.1016/S0168-9525(00)02024-2

1284 Rojas-Aedo, J. F., Gil-Durán, C., Goity, A., Vaca, I., Levicán, G., Larrondo, L. F., & Chávez, R.
1285 (2018). The developmental regulator Pcz1 affects the production of secondary metabolites in the
1286 filamentous fungus *Penicillium roqueforti*. *Microbiological Research*, *212–213*, 67–74.
1287 https://doi.org/10.1016/j.micres.2018.05.005

1288 Ropars, J., López-Villavicencio, M., Dupont, J., Snirc, A., Gillot, G., Coton, M., Jany, J.-L., Coton, E.,
1289 & Giraud, T. (2014). Induction of sexual reproduction and genetic diversity in the cheese fungus
1290 *Penicillium roqueforti*. *Evolutionary Applications*, *7*(4), 433–441. https://doi.org/10.1111/eva.12140

1291 Ropars, J., Rodríguez de la Vega, R. C., López-Villavicencio, M., Gouzy, J., Sallet, E., Dumas, É.,
1292 Lacoste, S., Debuchy, R., Dupont, J., Branca, A., & Giraud, T. (2015). Adaptive Horizontal Gene
1293 Transfers Between Multiple Cheese-Associated Fungi. *Current Biology*, *25*(19), 2562–2569.
1294 https://doi.org/10.1016/j.cub.2015.08.025

1295 Ropars, J., Toro, K. S., Noel, J., Pelin, A., Charron, P., Farinelli, L., Marton, T., Krüger, M., Fuchs, J.,
1296 Brachmann, A., & Corradi, N. (2016). Evidence for the sexual origin of heterokaryosis in arbuscular
1297 mycorrhizal fungi. Nature Microbiology, 1(6), 1–9. https://doi.org/10.1038/nmicrobiol.2016.33

1298 Ropars, J., Caron, T., Lo, Y.-C., Bennetot, B., & Giraud, T. (2020). The domestication of Penicillium
1299 cheese fungi. *Comptes Rendus - Biologies*, *1*(0). https://doi.org/10.5802/crbiol.15

1300 Ropars, J., & Giraud, T. (2022). Convergence in domesticated fungi used for cheese and dry-cured
1301 meat maturation: Beneficial traits, genomic mechanisms, and degeneration. *Current Opinion in*
1302 *Microbiology*, *70*, 102236. https://doi.org/10.1016/j.mib.2022.102236

1303 Schneider, C. A., Rasband, W. S., & Eliceiri, K. W. (2012). NIH Image to ImageJ: 25 years of image
1304 analysis. *Nature Methods*, *9*(7), 671–675. https://doi.org/10.1038/nmeth.2089

1305 Schuelke, M. (2000). An economic method for the fluorescent labeling of PCR fragments. A poor
1306 man's approach to genotyping for research and high-throughput diagnostics. *Nature Biotechnology*,
1307 *18*, 233–234. https://doi.org/10.1038/72708

1308 Scott, P. M. (1981). Toxins of *Penicillium* Species Used in Cheese Manufacture. *Journal of Food*
1309 *Protection*, *44*(9), 702–710. https://doi.org/10.4315/0362-028X-44.9.702

1310 Seekles, S. J., Teunisse, P. P. P., Punt, M., Van Den Brule, T., Dijksterhuis, J., Houbraken, J., Wösten,
1311 H. A. B., & Ram, A. F. J. (2021). Preservation stress resistance of melanin deficient conidia from
1312 *Paecilomyces variotii* and *Penicillium roqueforti* mutants generated via CRISPR/Cas9 genome editing.
1313 *Fungal Biology and Biotechnology*, *8*(1), 4. https://doi.org/10.1186/s40694-021-00111-w

1314 Silva, M. V. B., dos Santos, D. J. A., Boison, S. A., Utsunomiya, A. T. H., Carmo, A. S., Sonstegard,
1315 T. S., Cole, J. B., & Van Tassell, C. P. (2014). The development of genomics applied to dairy
1316 breeding. *Livestock Science*, *166*(1), 66–75. https://doi.org/10.1016/j.livsci.2014.05.017

1317 Smit, A., & Hubley, R. (2008). *RepeatModeler Open-1.0* (1.0) [Computer software].
1318 http://www.repeatmasker.org

1319 Smit, A., Hubley, R., & Green, P. (2013). *RepeatMasker Open-4.0*. (4.0) [Computer software].
1320 http://www.repeatmasker.org

1321 Solares, E. A., Chakraborty, M., Miller, D. E., Kalsow, S., Hall, K., Perera, A. G., Emerson, J. J., &
1322 Hawley, R. S. (2018). Rapid Low-Cost Assembly of the *Drosophila melanogaster* Reference Genome
1323 Using Low-Coverage, Long-Read Sequencing. *G3 Genes|Genomes|Genetics*, *8*(10), 3143–3154.
1324 https://doi.org/10.1534/g3.118.200162

1325 Somta, P., Chen, J., Yimram, T., Yundaeng, C., Yuan, X., Tomooka, N., & Chen, X. (2020). QTL
1326 Mapping for Agronomic and Adaptive Traits Confirmed Pleiotropic Effect of *mog* Gene in Black
1327 Gram [*Vigna mungo* (L.) Hepper]. *Frontiers in Genetics*, *11*, 635.
1328 https://doi.org/10.3389/fgene.2020.00635

1329 Stanke, M., Schöffmann, O., Morgenstern, B., & Waack, S. (2006). Gene prediction in eukaryotes
1330 with a generalized hidden Markov model that uses hints from external sources. BMC Bioinformatics,
1331 7(1), 62. https://doi.org/10.1186/1471-2105-7-62

1332 Stanke, M., Diekhans, M., Baertsch, R., & Haussler, D. (2008). Using native and syntenically mapped
1333 cDNA alignments to improve de novo gene finding. Bioinformatics, 24(5), 637–644.
1334 https://doi.org/10.1093/bioinformatics/btn013

1335 Steinmetz, L. M., Sinha, H., Richards, D. R., Spiegelman, J. I., Oefner, P. J., McCusker, J. H., &
1336 Davis, R. W. (2002). Dissecting the architecture of a quantitative trait locus in yeast. *Nature*,
1337 *416*(6878), 326–330. https://doi.org/10.1038/416326a

1338 Sweeney, M., & McCouch, S. (2007). The Complex History of the Domestication of Rice. *Annals of*
1339 *Botany*, *100*(5), 951–957. https://doi.org/10.1093/aob/mcm128

1340 Swinnen, S., Thevelein, J. M., & Nevoigt, E. (2012). Genetic mapping of quantitative phenotypic traits
1341 in *Saccharomyces cerevisiae*. *FEMS Yeast Research*, *12*(2), 215–227. https://doi.org/10.1111/j.1567-
1342 1364.2011.00777.x

1343 Tang, H., Zhang, X., Miao, C., Zhang, J., Ming, R., Schnable, J. C., Schnable, P. S., Lyons, E., & Lu,
1344 J. (2015). ALLMAPS: Robust scaffold ordering based on multiple maps. *Genome Biology*, *16*(1), 3.
1345 https://doi.org/10.1186/s13059-014-0573-1

1346 Taylor, J., & Butler, D. (2017). *R* Package ASMap: Efficient Genetic Linkage Map Construction and
1347 Diagnosis. *Journal of Statistical Software*, *79*(6). https://doi.org/10.18637/jss.v079.i06

1348 Telias, A., Lin-Wang, K., Stevenson, D. E., Cooney, J. M., Hellens, R. P., Allan, A. C., Hoover, E. E.,
1349 & Bradeen, J. M. (2011). Apple skin patterning is associated with differential expression of *MYB10*.
1350 *BMC Plant Biology*, *11*(1), 93. https://doi.org/10.1186/1471-2229-11-93

1351 Todd, R. T., Forche, A., & Selmecki, A. (2017). Ploidy Variation in Fungi—Polyploidy, Aneuploidy,
1352 and Genome Evolution. *Microbiology Spectrum*, *5*(4), 1–31.
1353 https://doi.org/10.1128/microbiolspec.FUNK-0051-2016.

1354 Torrent, C., Gil-Durán, C., Rojas-Aedo, J. F., Medina, E., Vaca, I., Castro, P., García-Rico, R. O.,
1355 Cotoras, M., Mendoza, L., Levicán, G., & Chávez, R. (2017). Role of *sfk1* Gene in the Filamentous
1356 Fungus *Penicillium roqueforti*. *Frontiers in Microbiology*, *8*, 2424.
1357 https://doi.org/10.3389/fmicb.2017.02424

1358 Turner, B. C., & Perkins, D. D. (1979). SPORE KILLER, A CHROMOSOMAL FACTOR IN
1359 NEUROSPORA THAT KILLS MEIOTIC PRODUCTS NOT CONTAINING IT. *Genetics*, *93*(3),
1360 587–606. https://doi.org/10.1093/genetics/93.3.587

1361 Untergasser, A., Cutcutache, I., Koressaar, T., Ye, J., Faircloth, B. C., Remm, M., & Rozen, S. G.
1362 (2012). Primer3-new capabilities and interfaces. *Nucleic Acids Research*, *40*(15), e115.
1363 https://doi.org/10.1093/nar/gks596

1364 Van Wyk, S., Harrison, C. H., Wingfield, B. D., De Vos, L., Van Der Merwe, N. A., & Steenkamp, E.
1365 T. (2019). The RIPper, a web-based tool for genome-wide quantification of Repeat-Induced Point
1366 (RIP) mutations. *PeerJ*, *7*, e7447. https://doi.org/10.7717/peerj.7447

1367 Vernozy-Rozand, C., Mazuy-Cruchaudet, C., Bavai, C., Montet, M. P., Bonin, V., Dernburg, A., &
1368 Richard, Y. (2005). Growth and survival of *Escherichia coli* O157:H7 during the manufacture and
1369 ripening of raw goat milk lactic cheeses. *International Journal of Food Microbiology*, *105*(1), 83–88.
1370 https://doi.org/10.1016/j.ijfoodmicro.2005.05.005

1371 Vion, C., Peltier, E., Bernard, M., Muro, M., & Marullo, P. (2021). Marker Assisted Selection of
1372 Malic-Consuming Saccharomyces cerevisiae Strains for Winemaking. Efficiency and Limits of a
1373 QTL's Driven Breeding Program. Journal of Fungi, 7(4), 304. https://doi.org/10.3390/jof7040304

1374 Walker, B. J., Abeel, T., Shea, T., Priest, M., Abouelliel, A., Sakthikumar, S., Cuomo, C. A., Zeng, Q.,
1375 Wortman, J., Young, S. K., & Earl, A. M. (2014). Pilon: An Integrated Tool for Comprehensive
1376 Microbial Variant Detection and Genome Assembly Improvement. *PLoS ONE*, *9*(11), e112963.
1377 https://doi.org/10.1371/journal.pone.0112963

1378 Wang, J., Liao, X., Li, Y., Zhou, R., Yang, X., Gao, L., & Jia, J. (2010). Fine mapping a
1379 domestication-related QTL for spike-related traits in a synthetic wheat. *Genome*, *53*(10), 798–804.
1380 https://doi.org/10.1139/G10-066

1381 Wei, T., & Simko, V. (2021). *R package "corrplot": Visualization of a Correlation Matrix* (0.92)
1382 [Computer software]. https://github.com/taiyun/corrplot

1383 Wick, R. R., Judd, L. M., Gorrie, C. L., & Holt, K. E. (2017). Completing bacterial genome assemblies
1384 with multiplex MinION sequencing. *Microbial Genomics*, *3*(10).
1385 https://doi.org/10.1099/mgen.0.000132

1386 Wicker, T., Sabot, F., Hua-Van, A., Bennetzen, J. L., Capy, P., Chalhoub, B., Flavell, A., Leroy, P.,
1387 Morgante, M., Panaud, O., Paux, E., SanMiguel, P., & Schulman, A. H. (2007). A unified
1388 classification system for eukaryotic transposable elements. *Nature Reviews Genetics*, *8*(12), 973–982.
1389 https://doi.org/10.1038/nrg2165

1390 Wickham, H. (2007). Reshaping Data with the {reshape} Package. *Journal of Statistical Software*,
1391 *21*(12), 1–20.

1392 Wickham, H. (2016). *ggplot2: Elegant Graphics for Data Analysis* [Computer software].
1393 https://ggplot2.tidyverse.org

1394 Wilkening, S., Lin, G., Fritsch, E. S., Tekkedil, M. M., Anders, S., Kuehn, R., Nguyen, M., Aiyar, R.
1395 S., Proctor, M., Sakhanenko, N. A., Galas, D. J., Gagneur, J., Deutschbauer, A., & Steinmetz, L. M.
1396 (2014). An Evaluation of High-Throughput Approaches to Qtl Mapping in *Saccharomyces Cerevisiae*.
1397 *Genetics*, *196*(3), 853–865. https://doi.org/10.1534/genetics.113.160291

1398 Wirén, A., & Jensen, P. (2011). A Growth QTL on Chicken Chromosome 1 Affects Emotionality and
1399 Sociality. *Behavior Genetics*, *41*(2), 303–311. https://doi.org/10.1007/s10519-010-9377-6

1400 Wright, D. (2015). The Genetic Architecture of Domestication in Animals. *Bioinformatics and*
1401 *Biology Insights*, *9S4*, BBI.S28902. https://doi.org/10.4137/BBI.S28902

1402 Wright, D., Rubin, C.-J., Martinez Barrio, A., Schütz, K., Kerje, S., Brändström, H., Kindmark, A.,
1403 Jensen, P., & Andersson, L. (2010). The genetic architecture of domestication in the chicken: Effects
1404 of pleiotropy and linkage. *Molecular Ecology*, *19*(23), 5140–5156. https://doi.org/10.1111/j.1365-
1405 294X.2010.04882.x

1406 Yao, J., Xu, J., Cornille, A., Tomes, S., Karunairetnam, S., Luo, Z., Bassett, H., Whitworth, C.,
1407 Rees□George, J., Ranatunga, C., Snirc, A., Crowhurst, R., De Silva, N., Warren, B., Deng, C., Kumar,
1408 S., Chagné, D., Bus, V. G. M., Volz, R. K., … Gleave, A. P. (2015). A *micro RNA* allele that emerged
1409 prior to apple domestication may underlie fruit size evolution. *The Plant Journal*, *84*(2), 417–427.
1410 https://doi.org/10.1111/tpj.13021

1411 Zimmer, A., Durand, C., Loira, N., Durrens, P., Sherman, D. J., & Marullo, P. (2014). QTL Dissection
1412 of Lag Phase in Wine Fermentation Reveals a New Translocation Responsible for *Saccharomyces*

cerevisiae Adaptation to Sulfite. *PLoS ONE*, *9*(1), e86298. https://doi.org/10.1371/journal.pone.0086298

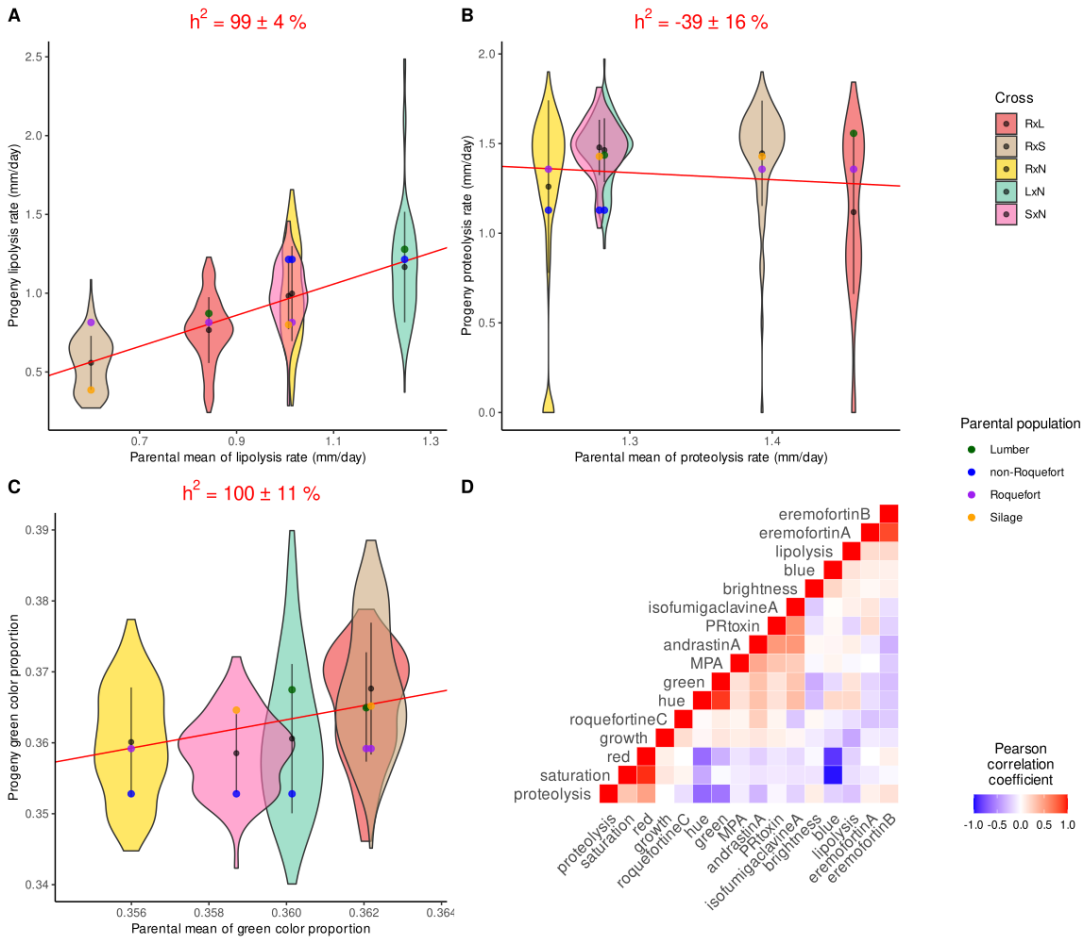

Figure 1: Distributions of phenotypes in the five progenies in *Penicillium roqueforti* as a function of their parental means, for (A) the lipolysis rate (mm/day), (B) the proteolysis rate (mm/day) and (C) the relative green color channel of the progeny; the parental means are plotted along the x axis (RxL in red, RxS in beige, RxN in yellow, LxN in turquoise and SxN in pink). The black point and line represent the mean and standard deviation, respectively, for each progeny. The colored points represent the parental values (lumber in green, non-Roquefort in blue, Roquefort in purple, silage in orange). The red line represents the linear regression across progenies, from which the slope is used to estimate the heritability (h^2) value given at the top. (D) Pearson correlation coefficients, as a color gradient, between trait values across offspring and crosses.

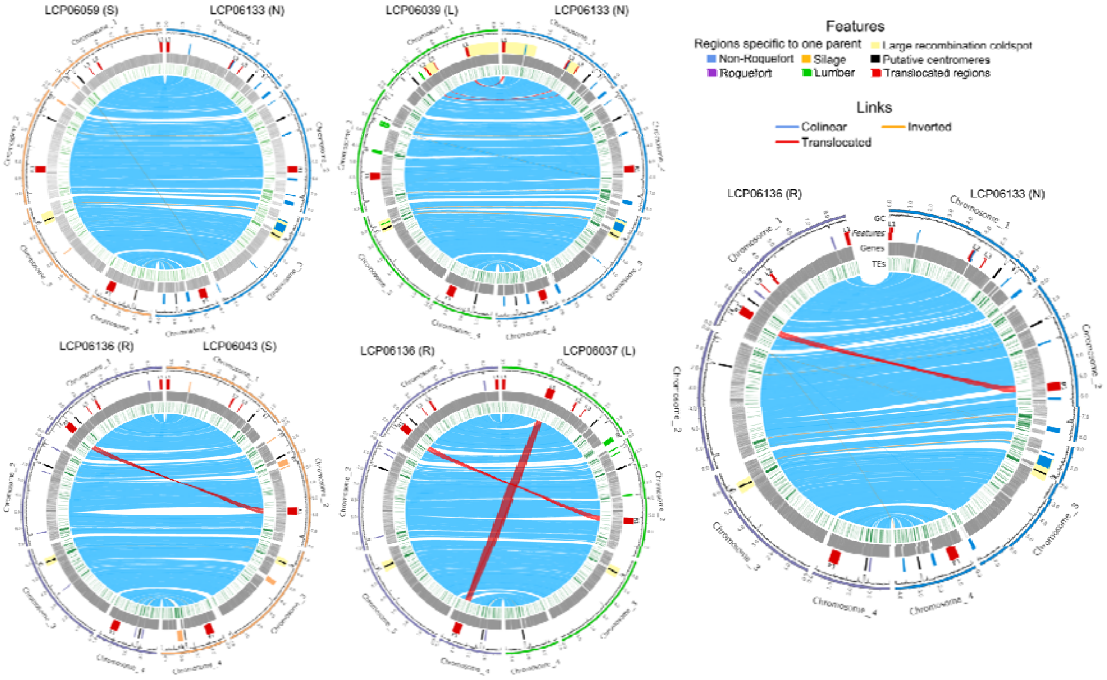

Figure 2: Genome comparisons between parental strains for each cross. Chromosomes are represented with colors corresponding to the population-of-origin of the strains: light orange, blue, purple and green for silage (S), non-Roquefort, (N) Roquefort (R) and lumber (L) populations, respectively. From outside to inside, the tracks represent the i) GC content, ii) translocated regions of more than 50kb between parental genomes in red (with their IDs, the first letter indicating the population-of-origin of the parent in which the translocation occurred), specific regions that are lacking in other genomes (*i.e.* acquired horizontally transferred regions) with their color indicating the populations in which they are present, putative centromeres in black, and large recombination cold spots in light yellow, iii) predicted genes in grey and iv) transposable elements in green. Orthologs between genomes are linked one to each other, with blue, orange and red links, indicating synteny, inversions or >50kb translocations, respectively.

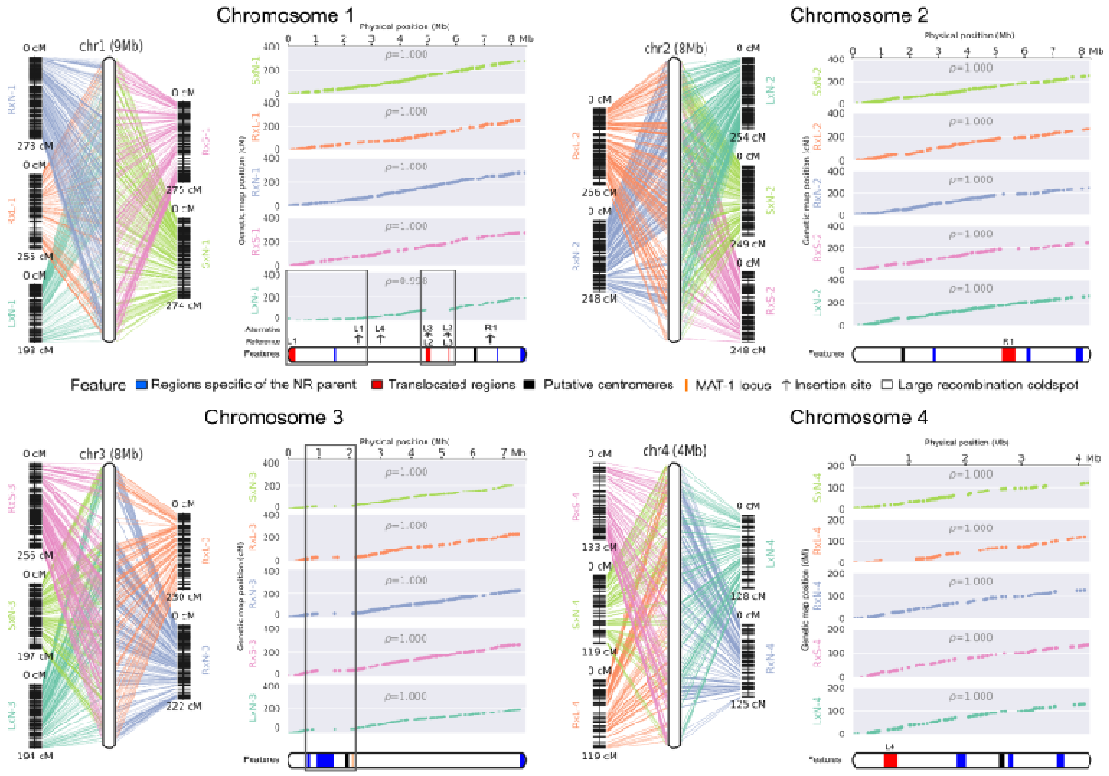

Figure 3: Genetic and physical maps for the four chromosomes of *Penicillium roqueforti*, obtained by analysing five inter-population crosses. Each panel corresponds to an individual chromosome, line graphs on the left represent linkage groups (one color per cross, with cross IDs as in Table 1; note that different parents were used for the silage and lumber populations between crosses); the lines link markers to chromosomes of the reference genome (LCP06133 non-Roquefort parent). In each panel, plots on the right represent the relationship between genetic and physical distance, with one plot per cross and the same color code as in left panels. At the bottom of each panel, the reference chromosome is represented, with filled black, red and blue rectangles representing the putative centromeres, the translocated regions and the horizontally transferred regions of more than 50kb when present, respectively. The red translocated regions are labelled as in Figure 2. The orange bar in chromosome 3 represents the mating-type locus position. The empty black rectangles indicate large recombination cold spots situated between translocated or parent-specific regions.

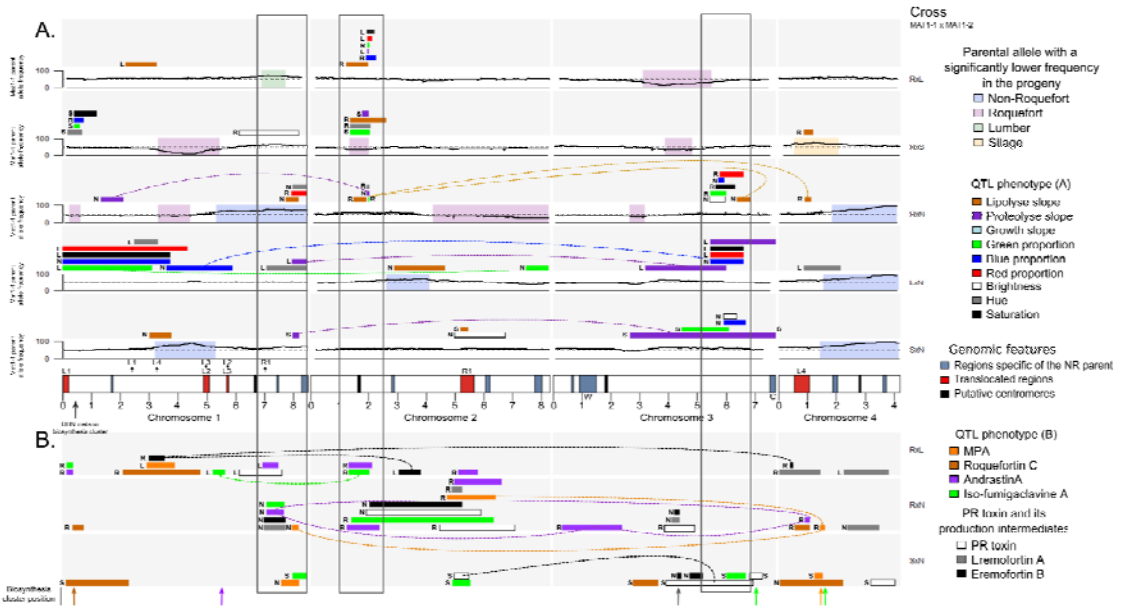

Figure 4: Representation of identified quantitative trait loci (QTLs) and segregation distortion along the four chromosomes of *Penicillium roqueforti* in five progenies. Only QTLs explaining more than 5% of the total variance are represented. The color of the bars indicates the considered trait while the letter indicates the parent having the alleles increasing the trait value. Dotted lines link the QTLs with significant interactions and color indicates the phenotype. The cross ID is indicated on the right, the first parent carrying the MAT1-1 mating type. (A) QTLs identified for phenotypes linked to lipolysis, proteolysis, growth and colony color for the five crosses (in lines, indicated on the right with the same code as in Table 1, note that different parents were used for the silage and lumber populations between crosses). Black curves represent the proportion in progenies of the allele from the parent carrying the MAT1-1 mating type. Transparent colored rectangles on curves indicate regions with significant segregation distortion, their color corresponding to the under-represented parental allele: blue, purple, green and yellow for non-Roquefort, Roquefort, lumber/spoiled food and silage/spoiled food parents, respectively. The x-axis represents genomic physical positions. At the bottom, the four chromosomes of the reference genome (LCP06133) are represented, with rectangles representing genomic features: large horizontally transferred regions specific to the reference genome in blue, and translocated regions in the reference genome in red (with same IDs as in Figure 2). The location of the horizontally

transferred regions (W for *Wallaby* and C for *CheesyTer*) are indicated. The location of the dihydroxynaphthalene (DHN) melanin production cluster is indicated by a black arrow. The large vertical empty black rectangles indicate pleiotropic QTL regions, with effects on multiple traits. (B) QTLs identified for extrolite production (with colors corresponding to the different toxins), analyzed in three crosses (SxN, RxN and LxN). The locations of the gene clusters of the toxin biosynthesis pathways are indicated by arrows with the same color code (the PR toxin cluster being in gray, eremofortin A and B being intermediates).

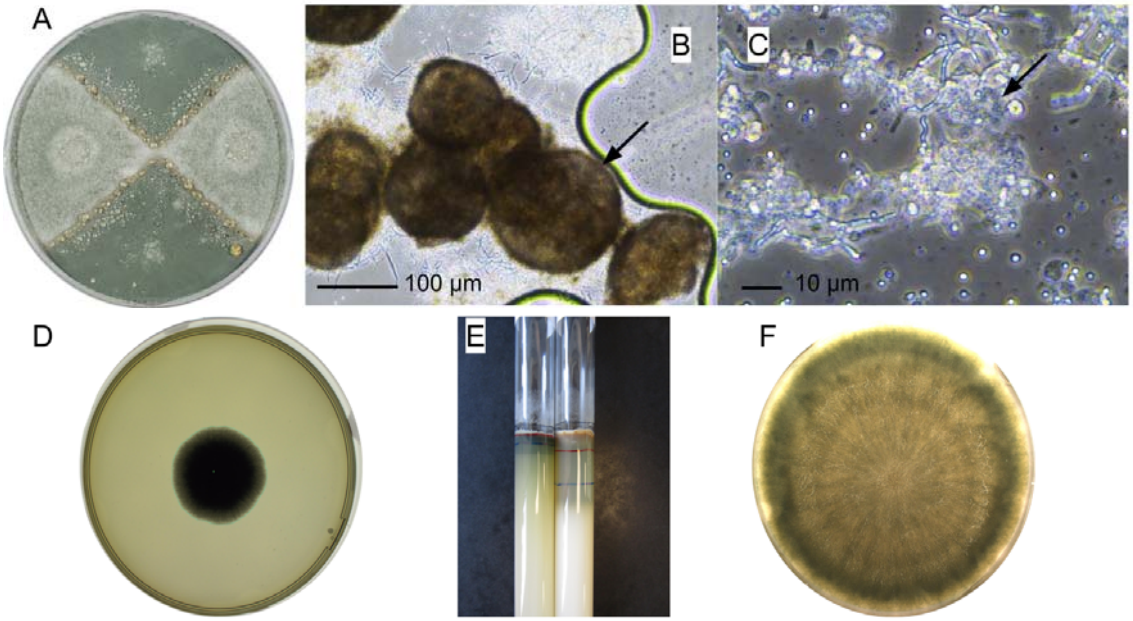

Figure 5: Observations of *Penicillium roqueforti* crosses and examples of phenotypic trait determination. (A) Petri dish with a cross between the LCP06136 (MAT1-1; Roquefort; at the top and bottom) and LCP06173 (MAT1-2; non-Roquefort; at left and right) strains. Sexual structures are formed at the contact zones between the two strains. (B) Cleistothecia (sexual structures of *Penicillium roqueforti*) shown by black arrow. (C) Asci containing ascospores shown by the black arrow. (D) Petri dish used for estimating colony growth rate, by counting the number of pixels occupied by the fungal colony (one offspring grown on malt medium for 120 hours). (E) Two lipolysis test tubes showing the lysis dynamics, for two different strains, with marks on the tubes indicating the limit of lipid medium

1490 degradation at different times (blue, red and blue marks, drawn at 0, 7 and 14 days, respectively). (F)

1491 Petri dish on which an offspring grew on raw sheep milk medium during 13 days for color measure.

1492

Table 1: The five crosses performed using six strains of *Penicillium roqueforti* from different populations (R for Roquefort, N for non-Roquefort, L for lumber/food spoiler, S for silage/food spoiler) with opposite mating types (MAT1-1 and MAT1-2), with the number of isolated and phenotyped offspring and the number of marker obtained from GBS genotyping. LCP: « Laboratoire de Cryptogamie, Paris ». *The strain LCP06039 was found to be a mixture of two morphotypes ("dark" and "light"), which was detected after the cross had been performed. ¤These offspring have been genotyped with indels, in addition to GBS, as all other offspring.

Cross	MAT1-1		MAT1-2		Ascospores isolated	Offspring GBS-genotyped	Offspring growth-phenotyped	Offspring color-phenotyped	Offspring lipolysis phenotyped	Offspring proteolysis phenotyped	Offspring phenotyped (mycotoxins)	Offspring used for map construction	Number of marker
	Population	Strain	Population	Strain									
RxN	Roquefort	LCP06136	non-Roquefort	LCP06133	389	384¤	307	311	387	382	274	358	2462
RxS	Roquefort	LCP06136	silage/food spoiler	LCP06043	157	157	157	157	157	156	0	148	2902
RxL	Roquefort	LCP06136	lumber/food spoiler	LCP06037	185	185	129	131	150	141	120	159	2943
SxN	silage/food spoiler	LCP06059	non-Roquefort	LCP06133	176	176	92	92	150	150	75	160	2860
LxN	lumber/food spoiler	LCP06039*	non-Roquefort	LCP06133	171	171	91	91	150	151	0	165	2618

Table 2: The five crosses performed using six strains of *Penicillium roqueforti* from different populations (R for Roquefort, N for non-Roquefort, L for lumber/food spoiler, S for silage/food spoiler), the linkage group and the total, the number of markers used for genetic map construction, the total length of the linkage group, the average and maximum spacing in cM between markers, the mean recombination rate in cM/Mb, and the reference chromosome and genome size in Mb.

Cross	Linkage group	Number of markers	Mean number of crossing over	Length (cM)	Average spacing (cM)	Maximum spacing (cM)	Mean recombination rate (cM/Mb)	Reference size (Mb)
SxN	L.1	213	2.74	274	1.3	8.8	32.21	8.51
	L.2	242	2.49	249	1	12.8	29.97	8.31
	L.3	189	1.97	197	1	8.8	25.51	7.72
	L.4	94	1.19	120	1.3	8.8	28.47	4.22
	overall	738	8.39	841	1.1	12.8	29.25	28.75
LxN	L.1	161	1.98	199	1.2	9.2	23.39	8.51
	L.2	248	2.55	255	1	9.2	30.69	8.31
	L.3	164	1.95	195	1.2	6.7	25.25	7.72
	L.4	103	1.28	128	1.3	8.6	30.36	4.22
	overall	676	7.75	776	1.2	9.2	26.99	28.75
RxN	L.1	466	2.78	279	0.6	7.3	32.79	8.51
	L.2	435	2.48	248	0.6	8.7	29.85	8.31
	L.3	378	2.22	223	0.6	9.6	28.88	7.72
	L.4	179	1.25	126	0.7	8.7	29.89	4.22
	overall	1458	8.74	875	0.6	9.6	30.43	28.75
RxS	L.1	191	2.74	275	1.4	11.7	32.32	8.51
	L.2	242	2.47	248	1	13.9	29.85	8.31
	L.3	227	2.55	256	1.1	12.4	33.15	7.72
	L.4	115	1.33	133	1.2	7.5	31.55	4.22
	overall	775	9.10	913	1.2	13.9	31.75	28.75
RxL	L.1	186	2.64	264	1.4	14.9	31.03	8.51
	L.2	295	2.66	267	0.9	13.5	32.14	8.31
	L.3	181	2.30	231	1.3	9.5	29.91	7.72
	L.4	129	1.19	119	0.9	12.9	28.23	4.22
	overall	791	8.79	881	1.1	14.9	30.64	28.75
Crosses mean	L.1	243.4	2.58	258.2	1.18	10.38	30.348	8.51
	L.2	292.4	2.53	253.4	0.9	11.62	30.5	8.31
	L.3	227.8	2.20	220.4	1.04	9.4	28.54	7.72
	L.4	124	1.25	125.2	1.08	9.3	29.7	4.22
	overall	887.6	8.55	857.2	1.04	12.08	29.812	28.75